NJC

PAPER

View Article Online
View Journal | View Issue

Cite this: *New J. Chem.*, 2019, **43**, 16396

Phenothiazine electrophores immobilized on periodic mesoporous organosilicas by ion exchange†

Björn Schäfgen,[a] Hilla Khelwati,[b] Dominique F. Bechtel,[a] Annelies DeCuyper,[a] Axel Schüssler,[a] Adam Neuba,[c] Antonio J. Pierik,[a] Stefan Ernst,‡[a] Thomas J. J. Müller *[b] and Werner R. Thiel *[a]

Received 10th September 2019,
Accepted 17th September 2019

DOI: 10.1039/c9nj04661e

rsc.li/njc

Two different phenothiazines carrying quaternary ammonium groups in the side chain have been synthesized and fully characterized. These compounds were immobilized by ion exchange on the surface of a periodic mesoporous organosilica (PMO) and a neat silica SBA-15 material bearing sulphonate groups covalently bound to the pore surface. The resulting porous and electrochromophoric materials were studied by means of solid state CP-MAS NMR, IR, UV/Vis and fluorescence spectroscopy, nitrogen adsorption/desorption measurements and cyclic voltammetry. Independent of the nature of the support, the colour of these materials changes to pink by irradiation with light, indicating the formation of phenothiazine radical cations. These species, which turned out to be highly stable even in the presence of atmospheric oxygen, were characterized by EPR spectroscopy.

1. Introduction

Fully reversible oxidation or reduction is rather associated with inorganic than with organic compounds. However, there are also some small, purely organic compounds showing this behaviour. During the past two decades, the phenothiazine motif became increasingly dominating for applications in organic electronics. Phenothiazines undergo a reversible one-electron oxidation at low potentials.[1] Fine-tuning of the redox potential is possible by choosing a suitable substitution pattern. The oxidation process results in stable and intensely coloured radical cations, which has widely been used for a quantitative determination of this class of compounds.[2] Based on their electronic properties, phenothiazines have gained multiple applications, not only in organic electronics but also in medicine,[3] biochemistry,[4] material sciences[5] or polymer chemistry.[6] In addition, the unusual combination of both luminescence and redox activity has made phenothiazines and their oligomers particularly interesting as redox switchable luminophores,[7] dye sensitizers in Grätzel-type solar cells,[8] and as donors in photoinduced intramolecular electron transfer systems.[9]

Some years ago these features motivated us to covalently immobilize phenothiazines in the pores of periodically structured mesoporous silica such as MCM-41.[10] Thereafter, a few reports of others dealing with phenothiazines on silica surfaces appeared.[11] We have particularly focused on materials with covalently grafted phenothiazines since simply adsorbed systems lack stability. Accordingly, different protocols for covalently grafting phenothiazines on silica-based materials with high specific surface areas were established. One critical point is the right choice of the linker between the phenothiazine core and the silica. Following the carbamate approach, commercially available 3-(triethoxysilyl)-propylisocyanate was reacted with a phenothiazine functionalized alcohol. Subsequently, the resulting product was covalently immobilized in the pores of MCM-41, by applying post-synthetic grafting. Oxidation with $(NO)BF_4$ resulted in long-lived, red-coloured, surface bound radical cations. However, according to this protocol, only about 15 wt% of the organic material could be ligated to the support. For higher loadings of phenothiazines inside the pores with a more homogeneous distribution of the redox-active sites along the pores, we had to switch to an *in situ* method. This means, that triethoxysilyl-functionalized phenothiazine precursors had to be applied in the reaction mixture for the formation of the support. This was not feasible with the carbamate linker since it is readily hydrolysed by the amine catalyst required for the support

[a] *Fachbereich Chemie, Technische Universität Kaiserslautern, Erwin-Schrödinger-Str. 54, D-67663 Kaiserslautern, Germany. E-mail: thiel@chemie.uni-kl.de*
[b] *Institut für Organische Chemie und Makromolekulare Chemie, Heinrich-Heine-Universität Düsseldorf, Universitätsstraße 1, D-40225 Düsseldorf, Germany. E-mail: ThomasJJ.Mueller@uni-duesseldorf.de*
[c] *Department Chemie, Universität Paderborn, Warburger Straße 100, D-33098 Paderborn, Germany*

† Electronic supplementary information (ESI) available: NMR, EPR, IR, UV/Vis and mass spectra, TGA and EDX data, SEM images. See DOI: 10.1039/c9nj04661e

‡ In memoriam to Prof. Dr Ing. Stefan Ernst who deceased on Jan. 28, 2019.

synthesis from tetraethoxysilane. To overcome this problem, urea based linkers were implemented. The corresponding triethoxysilyl-functionalized phenothiazine urea derivatives were therefore obtained by reacting amino-functionalized phenothiazines with 3-(triethoxysilyl)propylisocyanate. This strategy of *in situ* processing allowed increasing the loading to 30 wt% of organic material inside the pores while maintaining an acceptable quality of pore-ordering. Again one-electron oxidation gave red-coloured radical cations for monophenothiazines, while the oxidation of phenothiazine dyads resulted in green diradical dications. Finally solid state cyclic voltammetry proved that the reversible electrochemical oxidation of the surface-bound phenothiazine is possible.

We herein present a further development of the urea approach by using ionic end-groups that allow an electrostatic immobilization of the phenothiazine motif. We see a clear advantage in this approach providing a moderate mobility of phenothiazines along the pores, while keeping binding to the support. A phenylene-bridged periodic mesoporous organo silica of SBA 15 structure was used as the support here. Such materials possess more hydrophobic pore walls and a higher mechanical and chemical stability compared to neat silica supports. These properties are advantageous for using the materials in ion exchanging reactions.

2. Experimental

2.1. General considerations

All reactions leading to low-molecular-weight compounds were carried out under an inert atmosphere of nitrogen using septum and cannula techniques in heated one- or multi-necked flasks or Schlenk tubes. All reagents, catalysts and solvents were purchased reagent grade and used without further purification. THF, diethyl ether, dichloromethane, methanol and 1,4-dioxane were dried and distilled according to standard procedures. The phenothiazine derivatives **2**, **3**, **5**, BTEB (**11**) (1,4-(bistriethoxysilyl)benzene) and SBA-15 (**18**) were prepared according to procedures published in the literature.[12–14]

2.2. Spectroscopic characterization

The ^{1}H, ^{13}C and 135-DEPT NMR spectra were recorded on Bruker Avance III 300 and Avance III 600 instruments. The chemical ^{1}H NMR shifts δ are reported in ppm relative to the signals of the residual protons in the deuterated solvents (MeOH-d_4, acetone-d_6, or DMSO-d_6). In describing the multiplicity of the individual signals, the following common abbreviations were used: s (singlet), d (doublet), t (triplet), q (quartet), m (multiplet). In the description of the high resolution ^{13}C NMR spectra of the low-molecular-weight compounds primary carbon nuclei were designated with CH_3, secondary with CH_2, tertiary with CH, and quaternary with $C_{quat.}$. The assignments were made by using DEPT spectra. Solid-state ^{13}C CP-MAS NMR and ^{29}Si CP-MAS NMR spectra were recorded on a 500 MHz Bruker Avance III spectrometer with a spinning frequency of 11 000 Hz and resonance frequencies of 125 MHz and 99 MHz for ^{13}C or ^{29}Si nuclei, respectively. IR spectra for the low-molecular-weight compounds were recorded using a Shimadzu IRAffinity-1 device. An ATR-FT-IR spectrometer PerkinElmer Spectrum 100 containing a diamond coated ZnSe-window was used for measuring the infrared spectra of the PMOs with a spectral range of 4000–650 cm^{-1} and a resolution of ± 4 cm^{-1}. Intensities of the IR absorptions are indicated by w (weak), m (medium) and s (strong). The solid-state UV/Vis data were recorded on a PerkinElmer Lambda 18 UV/Vis spectrometer in a spectral range from 900–200 nm and with a step size of 1 nm. TGA analyses were performed on a Setaram SETSYS 16/18 TGA/DTG system. Elemental analyses were performed on a PerkinElmer Series II Analyzer 2400 and an Elementar Vario Micro Cube at the Microanalytical Laboratories of the Institut für Pharamazeutische Chemie, Heinrich-Heine-Universität, Düsseldorf, Germany and with an Elementar Vario Micro Cube in the Analytical Laboratories at the TU Kaiserslautern, Germany. For column chromatography and TLC, analytic silica gel 60, mesh 70–230 or 60 F_{254} silica gel plates were used. Electron capture ionization mass spectra were measured with a triple quadrupole mass spectrometer TSQ 7000 from Finnigan MAT. The measurements of the melting points were carried out with a B-540 Büchi melting point apparatus. EPR spectra were recorded with a Bruker Elexsys E580 X-band EPR spectrometer working in the perpendicular mode at room temperature coupled to a dielectric resonator ER 4118X-5-MD (Bruker). The samples were measured in capillary tubes with a microwave frequency of 9.72 $\pm$ 0.01 GHz and a microwave power of 0.2–20 mW. The standard modulation amplitude for these radical compounds was 0.1–0.25 mT based on the spectral resolution of the sample.

2.3. Textural properties

X-Ray powder diffraction (PXRD) patterns of the silica samples were recorded on a Siemens/Bruker AXS Type D 5005 instrument using Cu-Kα radiation (λ = 0.15405 nm) in a 2Θ range of $0.5^\circ < 2\Theta < 5^\circ$ with a step range of 0.04°. N_2-adsorption–desorption isotherms, pore size distributions as well as additional textural properties of the materials were determined at -196 °C by a Quantachrome Autosorb-1-Instrument sorption analyser. Before analysis, the samples were degassed at 150 °C for at least 12 h under vacuum and then the adsorption–desorption procedure was conducted by passing nitrogen into the sample, which was kept under liquid nitrogen. The average pore sizes of the samples were estimated using the BJH approach based on the Kelvin equation while assuming a cylindrically shaped porous structure. The specific surface areas were calculated by means of the Brunauer–Emmett–Teller (BET) equation and the pore size distribution curves were analysed with the adsorption branch by the BJH method. The scanning electron microscope (SEM) images were taken on a Jeol JSM 6490 LA field emission device with acceleration voltage of 15 kV. The silica particles were deposited from suspension onto silicon wafers and thin Au films (approx. 10 nm) were deposited on the samples for imaging.

2.4. Electrochemistry

Cyclic voltammetry measurements of the low-molecular-weight compounds were carried out in a small volume glass cell (4 mL)

with a three electrode arrangement. The experiments were performed under argon atmosphere in dry and degassed dichloromethane at room temperature at scan rates of 100, 250, 500 and 1000 mV s^{-1}. The electrolyte was Bu_4NPF_6 (0.025 M). The working electrode was a 1 mm platinum disk, the counter electrode was a platinum wire and the reference electrode was an Ag/AgCl electrode. All potentials were corrected to the internal standard of decamethylferrocene/ferrocenium in dichloromethane ($E_0^{0/+1} = -0.095$ V). The cyclic and square-wave voltammetry measurements of the materials containing immobilized phenothiazines were performed with the Metrohm-Autolab potentiostat PGSTAT 101 in a CH_2Cl_2 or MeCN/0.1 M $^tBu_4NPF_6$ solution with the following three electrode arrangement: GC working electrode (d = 2 mm), Ag/0.01 M $AgNO_3$/MeCN-reference electrode and platinum wire counter electrode. For these measurements, the materials were deposited on the GC working electrode as follows: 2–4 mg of the material were suspended in water or ethanol and sonicated for several minutes. One small drop of the fine dispersion was placed on the GC electrode tip (d = 2 mm) and heated for 30 min at 80 °C to evaporate the solvent. All measurements were carried out under argon atmosphere, with absolute and vented solvents.

2.5. Synthetic procedures

***N*,*N*,*N*-Trimethyl-3-(10*H*-phenothiazin-10-yl)propan-1-ammonium trifluoromethanesulphonate (4).** 3-(10*H*-Phenothiazin-10-yl)propan-1-amine (**3**) (317 mg, 1.23 mmol) and potassium carbonate (1.71 g, 12.3 mmol) were suspended in methanol (12 mL) and methyl trifluoromethylsulphonate (1.35 mL, 12.3 mmol) was added dropwise to the solution while a colour change from orange to yellow could be observed. The reaction was stirred at room temp for 30 min and afterwards at 60 °C for 16 h. All volatile components were removed under reduced pressure, while the residue was dissolved in dichloromethane and filtrated from the residual solid. The solvent was removed under reduced pressure and the product was suspended in diethyl ether (2 × 12 mL). The product was dried under high vacuum and was obtained as a colourless powder (332 mg, 1.11 mmol, 90%). Mp 168–170 °C. R_f (methanol) 0.31. ^{1}H NMR (300 MHz, MeOH) δ 7.25 (m_c, 2 H), 7.19 (dd, ^3J = 7.6 Hz, ^4J = 1.6 Hz, 2 H), 7.06 (dd, ^3J = 8.1 Hz, ^4J = 0.9 Hz, 2 H), 6.99 (m_c, 2 H), 4.11 (t, ^3J = 6.3 Hz, 2 H), 3.45 (m_c, 2 H), 3.01 (s, 9 H), 2.25 (m_c, 2 H). ^{13}C NMR (125 MHz, MeOH) δ 146.2 ($C_{quat.}$), 128.8 (CH), 128.6 (CH), 127.4 ($C_{quat.}$), 124.3 (CH), 117.3 (CH), 65.7 (CH_2), 53.5 (CH_3), 44.7 (CH_2), 21.8 (CH_2). IR $\tilde{\nu}$ [cm^{-1}] 3065 (vw), 3042 (vw), 2965 (vw), 2868 (vw), 1593 (w), 1570 (w), 1485 (m), 1479 (m), 1460 (s), 1445 (m), 1422 (w), 1400 (w), 1339 (w), 1254 (vs), 1221 (s), 1200 (w), 1157 (s), 1140 (s), 1128 (m), 1109 (w), 1028 (s), 961 (w), 939 (w), 918 (w), 908 (w), 764 (s), 754 (w), 729 (m), 637 (s). MS (EI) m/z (%) 448 (1, $[C_{19}H_{23}F_3O_3N_2S_2]^+$), 299 (10, $[C_{18}H_{23}N_2S]^+$) 284 (41, $[C_{17}H_{20}N_2S]^+$), 239 (100, $[C_{15}H_{14}NS]^+$), 212 (18, $[C_{13}H_{10}NS]^+$), 199 (50, $[C_{12}H_8NS]^+$). Anal. calcd for $C_{18}H_{23}N_2S$ [299.5] C 50.88, H 5.17, N 6.25, S 14.30; found C 50.83, H 5.36, N 6.09, S 14.05.

3-(3,7-Dibromo-10*H*-phenothiazin-10-yl)propanenitrile (6). To an ice cooled suspension of 3,7-dibromo-10*H*-phenothiazine (**5**) (37.4 g, 104 mmol) in acrylonitrile (214 mL, 3.23 mol) a solution of Triton B (40 wt%, 3.83 mL, 22.0 μmol) was added dropwise under vigorous stirring. After complete addition, the solution was stirred at 0 °C for 5 min and a colour change from ochre to brown was observed. TLC indicated the completion of the reaction. The excessive acrylonitrile was removed under reduced pressure and the crude product was adsorbed onto Celite® and purified by column chromatography on silica gel (hexane/acetone 8 : 2). The product was obtained as a colourless, fluffy powder (31.2 g, 75.9 mmol, 74%). Mp 146–148 °C. R_f (hexane/acetone, 8 : 2) 0.26. ^{1}H NMR (600 MHz, DMSO) δ 7.42 (d, ^4J = 2.3 Hz, 2 H), 7.39 (dd, ^3J = 8.7 Hz, ^4J = 2.3 Hz, 2 H), 7.04 (d, ^3J = 8.7 Hz, 2 H), 4.18 (t, ^3J = 6.6 Hz, 2 H), 2.90 (t, ^3J = 6.6 Hz, 2 H). ^{13}C NMR (125 MHz, DMSO) δ 142.9 ($C_{quat.}$), 130.3 (CH), 129.2 (CH), 126.1 (C_{quat}), 118.4 ($C_{quat.}$), 117.7 (CH), 114.6 ($C_{quat.}$), 42.5 (CH_2), 15.7 (CH_2). IR $\tilde{\nu}$ [cm^{-1}] 3086 (vw), 2990 (vw), 2961 (vw), 2905 (vw), 2648 (vw), 2249 (vw), 1867 (vw), 1846 (vw), 1585 (vw), 1477 (w), 1452 (s), 1408 (w), 1391 (w), 1335 (m), 1317 (m), 1288 (w), 1248 (m), 1227 (w), 1194 (m), 1165 (w), 1155 (w), 1113 (w), 1096 (w), 1080 (w), 1070 (w), 1045 (w), 1028 (vw), 989 (vw), 901 (vw), 864 (m), 797 (s), 789 (m), 752 (m), 741 (w), 700 (vw), 650 (w), 606 (w). MS (EI) m/z (%) 412 (37, $[C_{15}H_{10}{}^{81}Br_2N_2S]^+$), 410 (81, $[C_{15}H_{10}{}^{79}Br^{81}BrN_2S]^+$), 408 (37, $[C_{15}H_{10}Br_2{}^{79}N_2S]^+$), 372 (52, $[C_{13}H_8{}^{81}Br_2NS]^+$), 370 (100, $[C_{13}H_8{}^{79}Br^{81}BrNS]^+$), 368 (48, $[C_{13}H_8{}^{79}Br_2NS]^+$), 358 (44, $[C_{12}H_6{}^{81}Br_2NS]^+$), 356 (89, $[C_{12}H_6{}^{79}Br^{81}BrNS]^+$), 354 (42, $[C_{12}H_6{}^{79}Br_2NS]^+$), 291 (59, $[C_{13}H_8{}^{81}BrNS]^+$), 289 (54, $[C_{13}H_8{}^{79}BrNS]^+$), 196 (65, $[C_{12}H_6NS]^+$).

3-(3,7-Dibromo-10*H*-phenothiazin-10-yl)propan-1-amine (7). Anhydrous indium trichloride (3.31 g, 15.0 mmol) and sodium borohydride (1.70 g, 45.0 mmol) were stirred in THF (50 mL) at room temp for 1 h, whereas a colour change from greenish to greyish could be observed. Afterwards, compound **6** (6.15 g, 15.0 mmol) was added to the reaction mixture which was stirred at room temp for another 4 h. The solution was quenched by the dropwise addition of 3 M hydrochloric acid (50 mL) and stirred under reflux for 1 h. Afterwards methanol (25 mL) was added and the solution was stirred again under reflux for 1 h. The organic solvents were removed under reduced pressure and the remaining aqueous solution was extracted with diethyl ether (50 mL). The acidic, aqueous solution was then adjusted with sodium hydroxide to pH 10 and the product was extracted with diethyl ether (3 × 50 mL). The combined organic phases were dried with anhydrous magnesium sulphate and the solvents were removed under reduced pressure while the crude product was adsorbed onto Celite®. After purification by column chromatography on silica gel (gradient of hexane/acetone 9 : 1 with 1% triethylamine to 7 : 3 with 1% triethylamine), the product was obtained as a greenish powder (6.09 g, 13.5 mmol, 91%). Mp 141 °C. R_f (hexane/acetone 1 : 1 with 1% triethylamine) 0.42. ^{1}H NMR (300 MHz, DMSO-d_6) δ 7.93 (s, 3 H), 7.47–7.35 (m, 4 H), 7.02 (d, ^3J = 8.9 Hz, 2 H), 3.95 (t, ^3J = 6.9 Hz, 2 H), 2.92–2.78 (m, 2 H), 1.94 (tt, ^3J = 7.2 Hz, 6.9 Hz, 2 H). ^{13}C NMR (150 MHz, DMSO-d_6) δ 143.6 ($C_{quat.}$), 130.4 (CH), 129.2 (CH), 125.9 ($C_{quat.}$), 117.9 (CH), 114.4 ($C_{quat.}$), 43.9 (CH_2), 36.5 (CH_2), 24.3 (CH_2). IR $\tilde{\nu}$ [cm^{-1}] 3092 (vw), 3057 (vw), 2934 (vw), 2872 (vw), 1585 (w), 1479 (m), 1456 (s), 1387 (w), 1327 (w), 1294 (w), 1252 (m), 1229

(m), 1150 (w), 1109 (w), 1082 (w), 1057 (w), 868 (w), 806 (m), 750 (m), 650 (w). MS (EI) *m*/*z* (%) 416 (36, $[C_{15}H_{14}{}^{81}Br_2N_2S]^+$), 414 (70, $[C_{15}H_{14}{}^{79}Br^{81}BrN_2S]^+$), 412 (34, $[C_{15}H_{14}{}^{79}Br_2N_2S]^+$), 398 (20, $[C_{15}H_{12}{}^{81}Br_2NS]^+$), 396 (39, $[C_{15}H_{12}{}^{79}Br^{81}BrNS]^+$), 394 (19, $[C_{15}H_{12}{}^{79}Br_2NS]^+$), 372 (12, $[C_{13}H_8{}^{81}Br_2NS]^+$), 370 (24, $[C_{13}H_8{}^{79}Br^{81}BrNS]^+$), 368 (12, $[C_{13}H_8{}^{79}Br_2NS]^+$), 358 (48, $[C_{12}H_6{}^{81}Br_2NS]^+$), 356 (85, $[C_{12}H_6{}^{79}Br^{81}BrNS]^+$), 354 (42, $[C_{12}H_6{}^{79}Br_2NS]^+$), 291 (21, $[C_{13}H_8{}^{81}BrNS]^+$), 289 (20, $[C_{13}H_8{}^{79}BrNS]^+$), 277 (29, $[C_{12}H_6{}^{81}BrNS]^+$), 196 (73, $[C_{12}H_6NS]^+$).

***tert*-Butyl-(3-(3,7-dibromo-10*H*-phenothiazin-10-yl)propyl)-carbamate (8).** Compound **7** (4.28 g, 9.60 mmol), triethylamine (2.63 mL, 19.2 mmol) and di-*tert*-butyl dicarbonate (2.51 g, 11.5 mmol) were dissolved in dichloromethane (9.6 mL) and 4-dimethylaminopyridine (116 mg, 0.96 mmol, 10 mol%) was added in small portions to the reaction mixture. After a reaction time of 1 h at 40 °C the solvent was evaporated, the crude product was adsorbed onto Celite® and purified by column chromatography on silica gel (hexane/acetone 8 : 2). The product was isolated as yellow crystals (4.36 g, 8.45 mmol, 88%). Mp 70–72 °C. R_f (hexane/acetone 7 : 3 with 1% triethylamine) 0.39. ^{1}H NMR (300 MHz, DMSO-d$_6$) δ 7.38–7.33 (m, 4 H), 6.96 (d, ^3J = 7.7 Hz, 2 H), 6.86 (t, ^3J = 4.9 Hz, 1 H), 3.83 (t, ^3J = 6.5 Hz, 2 H), 3.01 (m, 2 H), 1.76 (m, 2 H), 1.35 (s, 9 H). ^{13}C NMR (75 MHz, DMSO-d$_6$) δ 155.6 ($C_{quat.}$), 143.8 ($C_{quat.}$), 130.3 (CH), 129.1 (CH), 125.6 ($C_{quat.}$), 117.6 (CH), 114.1 ($C_{quart.}$), 77.5 ($C_{quat.}$), 44.5 (CH_2), 37.6 (CH_2), 28.2 (CH_3), 26.4 (CH_2). IR $\tilde{\nu}$ [cm^{-1}] 3395 (vw), 3379 (vw), 2976 (w), 2926 (w), 2868 (vw), 2851 (vw), 1694 (m), 1686 (m), 1516 (w), 1506 (m), 1481 (w), 1452 (vs), 1389 (m), 1364 (m), 1327 (w), 1267 (m), 1248 (s), 1202 (w), 1163 (s), 1109 (w), 1082 (w), 1040 (vw), 1003 (w), 959 (vw), 932 (vw), 868 (m), 802 (s), 779 (w), 750 (m), 652 (w). MS (EI) *m*/*z* (%) 516 (14, $[C_{20}H_{22}{}^{81}Br_2N_2O_2S]^+$), 514 (32, $[C_{20}H_{22}{}^{79}Br^{81}BrN_2O_2S]^+$), 512 (14, $[C_{20}H_{22}{}^{79}Br_2N_2O_2S]^+$), 460 (13, $[C_{16}H_{14}{}^{81}Br_2N_2O_2S]^+$), 458 (29, $[C_{16}H_{14}{}^{79}Br^{81}BrN_2O_2S]^+$), 456 (13, $[C_{16}H_{14}{}^{79}Br_2N_2O_2S]^+$), 357 (62, $[C_{12}H_7{}^{79}Br^{81}BrNS]^+$), 277 (30, $[C_{12}H_7{}^{79}BrNS]^+$), 196 (39, $[C_{12}H_6NS]^+$), 102 (100, $[C_5H_9O_2]^+$). Anal. calcd for $C_{20}H_{22}Br_2N_2O_2S$ [514.3] C 46.71, H 4.31, N 5.45, S 6.23; found C 46.98, H 4.17, N 5.32, S 6.23.

***tert*-Butyl-(3-(3,7-di(thiophen-2-yl)-10*H*-phenothiazin-10-yl)-propyl)carbamate (9).** Compound **8** (514 mg, 1.00 mmol), 4,4,5,5-tetramethyl-2-(thiophen-2-yl)-1,3,2-dioxaborolane (462 mg, 2.20 mmol), caesium fluoride (973 mg, 6.40 mmol) and tetrakis-(triphenylphosphane)palladium(0) (69 mg, 0.06 mmol, 6 mol%) were suspended in 1,4-dioxane (10 mL) and the reaction mixture was stirred under reflux for 14 h. After cooling to room temp the solvent was removed under reduced pressure, the residue was adsorbed onto Celite® and was purified by column chromatography on silica gel (hexane/acetone 8 : 2). The product could be isolated as yellow crystals (401 mg, 770 μmol, 77%). Mp 138–141 °C. R_f (hexane/acetone, 7 : 3) 0.34. ^{1}H NMR (600 MHz, DMSO) δ 7.48 (dd, ^3J = 5.1 Hz, ^4J = 1.1 Hz, 2 H), 7.46–7.42 (m, 6 H), 7.04 (dd, ^3J = 9.1 Hz, 2 H), 7.04 (d, ^3J = 9.1 Hz, 2 H), 6.92 (t, ^3J = 5.5 Hz, 1 H), 3.91 (t, ^3J = 7.0 Hz, 2 H), 3.07 (m_c, 2 H), 1.84 (m_c, 2 H), 1.36 (s, 9 H). ^{13}C NMR (75 MHz, DMSO-d$_6$) δ 155.6 ($C_{quat.}$), 143.4 ($C_{quat.}$), 142.2 ($C_{quat.}$), 128.5 ($C_{quat.}$), 128.5 (CH), 125.0 (CH), 124.9 (CH), 123.7 (CH), 123.6 ($C_{quat.}$), 123.1 (CH), 116.1 (CH), 77.5 ($C_{quat.}$), 44.5 (CH_2), 37.7 (CH_2), 28.3 (CH_3), 26.6 (CH_2). IR $\tilde{\nu}$ [cm^{-1}] 2974 (w), 2926 (w), 2864 (w), 1701 (m), 1680 (m), 1472 (vs), 1429 (m), 1400 (m), 1391 (m), 1364 (m), 1348 (w), 1333 (w), 1292 (w), 1261 (s), 1238 (s), 1207 (m), 1163 (s), 1109 (m), 1080 (w), 1042 (w), 1020 (w), 1007 (vw), 988 (w), 951 (vw), 951 (vw), 874 (m), 851 (m), 810 (s), 793 (m), 783 (w), 750 (m), 691 (vs), 650 (vw). MS (EI) *m*/*z* (%) 520 (32, $[C_{28}H_{28}N_2O_2S_3]^+$), 464 (24, $[C_{24}H_{19}N_2O_2S_3]^+$), 446 (6, $[C_{24}H_{19}N_2OS_3]^+$), 420 (13, $[C_{23}H_{19}N_2S_3]^+$), 376 (8, $[C_{21}H_{14}NS_3]^+$), 362 (100, $[C_{20}H_{12}NS_3]^+$). Anal. calcd for $[C_{28}H_{28}N_2O_2S_3]$ [519.7] C 64.58, H 5.42, N 5.38, S 18.47; found C 64.83, H 5.69, N 5.12, S 18.17.

3-(3,7-Di(thiophen-2-yl)-10*H*-phenothiazin-10-yl)-*N*,*N*,*N*-trimethylpropan-1-ammonium trifluoromethanesulphonate (10). Compound **9** (200 mg, 385 μmol) was dissolved in dichloromethane (3.8 mL) and trifluoroacetic acid (237 μL, 3.08 mmol) was added to the solution. The reaction mixture was stirred at 40 °C for 16 h. Volatile components were removed under reduced pressure and the residue was dissolved in methanol (3.8 mL). Potassium carbonate (530 mg, 3.85 mmol) and methyl trifluoromethylsulphonate (630 mg, 3.85 mmol) were added and the reaction mixture was stirred at room temp for 30 min and afterwards at 60 °C for 16 h. The evaporable components were removed under reduced pressure and the crude product was adsorbed onto aluminium oxide and purified by column chromatography on aluminium oxide (gradient of dichloromethane to dichloromethane/methanol 3%). The product could be obtained as yellow powder (181 mg, 296 mmol, 77%). Mp 128–130 °C. R_f (methanol) 0.10. ^{1}H NMR (600 MHz, DMSO) δ 7.52–7.49 (m, 4 H), 7.43 (dd, ^3J = 5.1 Hz, ^3J = 0.9 Hz, 2 H), 7.16 (d, ^3J = 8.3 Hz, 2 H), 7.11 (m_c, 2 H), 7.04 (dd, ^3J = 3.6 Hz, ^3J = 1.1 Hz, 2 H), 4.21 (t, ^3J = 6.9 Hz, 2 H), 3.80 (m_c, 2 H), 3.05 (s, 9 H), 2.50 (m_c, 2 H). ^{13}C NMR (125 MHz, MeOH-d$_4$) δ 145.1 ($C_{quat.}$), 144.1 ($C_{quat.}$), 131.5 ($C_{quat.}$), 129.2 (CH), 127.5 ($C_{quat.}$), 126.4 (CH), 125.6 (CH), 125.6 (CH), 123.9 (CH), 117.6 (CH), 65.8 (CH_2), 53.7 (CH_3), 45.0 (CH_2), 22.0 (CH_2). IR: $\tilde{\nu}$ [cm^{-1}] 3034 (vw), 2963 (w), 1603 (vw), 1472 (s), 1427 (m), 1402 (m), 1346 (w), 1339 (w), 1258 (vs), 1223 (m), 1200 (w), 1153 (m), 1084 (s), 1045 (s), 1028 (vs), 1015 (s), 966 (w), 943 (vw), 910 (w), 872 (m), 851 (m), 799 (vs), 752 (m), 737 (w), 692 (s), 662 (vw), 637 (s), 610 (w). ESI-HRMS calcd for $[C_{26}H_{27}N_2S_3^+]$ 463.1336; found 463.1336.

BTEB-PMO (12). P123 (39.4 g, 6.79 mmol) was dissolved in a mixture of water (1.40 L) and concentrated hydrochloric acid (7.92 mL). The solution was stirred at room temp for 2 h. After this time it was cooled to 5 °C and BTEB (**11**) (40.0 g, 99.3 mmol) was added and the temperature of the reaction mixture was kept under 5 °C for 1 h. Then the temperature was raised to 40 °C and the stirring was continued for another 4 h whereby a colourless solid precipitated. After keeping the colourless suspension at 100 °C for additional 24 h without stirring, the white solid was filtered off and washed to neutral pH with water. To improve the pore structure the material was suspended in a closed vessel in water (800 mL) and kept at 100 °C without stirring for 24 h. To remove the template, the solid was first filtered off and then suspended in a mixture of ethanol (1.2 L) and concentrated hydrochloric acid (12 mL) and stirred under reflux for 18 h. The colourless solid was filtered off, washed with ethanol (2 × 400 mL) and diethyl ether (2 × 400 mL) and

then dried under vacuum. The latter procedure of template elimination was repeated two more times. The colourless solid was finally dried to constant weight yielding 21.9 g. ^{13}C CP-MAS NMR (125 MHz) δ 131.9, 67.8, 55.8, 14.0. ^{29}Si CP-MAS NMR (99 MHz) δ −65.9, −72.8, −80.7. PXRD 0.66 (s), 1.29 (w), 1.52 (w). BET $A_{spec.}$ (m^2 g^{-1}) 1066; total pore volume (BJH, cm^3 g^{-1}) 1.37; pore diameter (BJH, Å) 56.3. IR (ATR) $\tilde{\nu}$ [cm^{-1}] 3377 (w), 3059 (w), 2978 (w), 2893 (w), 1387 (w), 1151 (s), 1050 (s), 1021 (s), 926 (m), 780 (m). UV/Vis (nm) 230, 270, 276. Anal. found C 41.36, H 4.58.

SH-BTEB-PMO (13). In a typical grafting reaction **12** (5.00 g) and 3-MPTS (25.0 g, 121 mmol) were suspended in toluene (33 mL) and stirred under heating to reflux for 72 h. After cooling to room temp the product was filtered off, washed with toluene (3 × 50 mL) and dried at 70 °C for 18 h to give 6.09 g of a colourless solid. ^{13}C CP-MAS NMR (125 MHz) δ 132.5, 68.0, 56.5, 46.0, 25.4, 14.3, 9.8, 7.2. ^{29}Si CP-MAS NMR (99 MHz) δ −50.4, −60.5, −72.7, −81.0. PXRD 0.68 (s), 1.29 (w), 1.51 (w). BET $A_{spez.}$ (m^2 g^{-1}) 827; total pore volume (BJH, cm^3 g^{-1}) 1.10; pore diameter (BJH, Å) 56.1. IR (ATR) $\tilde{\nu}$ (cm^{-1}) 3375 (w), 2976 (w), 1384 (w), 1148 (m), 1034 (s), 1019 (s), 915 (m), 807 (w), 780 (m). UV/Vis (nm) 229, 271, 277. Anal. found C 38.89, H 4.86, S 4.09.

SH-BTEB-PMO (13). In a typical grafting reaction **12** (5.00 g) and 3-MPTS (25.0 g), 121 mmol, (3-mercaptopropyl)trimethoxysilane were suspended in toluene (33 mL) and stirred under heating to reflux for 72 h. After cooling to room temp the product was filtered off, washed with toluene (3 × 50 mL) and dried at 70 °C for 18 h to give 6.09 g of a colourless solid. ^{13}C CP-MAS NMR (125 MHz) δ 132.5, 68.0, 56.5, 45.75, 25.4, 13.9, 9.8. ^{29}Si CP-MAS NMR (99 MHz) δ −50.1, −60.4, −72.7, −81.0. PXRD 0.68 (s), 1.29 (w), 1.51 (w). BET $A_{spec.}$ (m^2 g^{-1}) 827; total pore volume (BJH, cm^3 g^{-1}) 1.10; pore diameter (BJH, Å) 56.1. IR (ATR) $\tilde{\nu}$ (cm^{-1}) 3375 (w), 2976 (w), 1384 (w), 1148 (m), 1034 (s), 1019 (s), 915 (m), 807 (w), 780 (m). UV/Vis (nm) 229, 271, 277. Anal. found C 38.89, H 4.86, S 4.09.

SO_3H-BTEB-PMO (14). The thiopropyl functionalized PMO **13** (1.00 g) was suspended in H_2O_2 (35%, 100 mL) and the mixture was stirred at 60 °C for 24 h. The product was filtered off and washed with water (100 mL) and ethanol (100 mL). The resulting colourless solid was dried at 60 °C for 18 h to give 0.86 g of a colourless solid. ^{13}C CP-MAS NMR (125 MHz) δ 131.5, 125.8, 68.0, 55.8, 51.8, 16.4, 14.0, 9.9. ^{29}Si CP-MAS NMR (99 MHz) δ −62.7, −72.5, −81.7, −95.1, −101.9. PXRD 0.72 (s), 1.36 (w), 1.61 (w). BET $A_{spec.}$ (m^2 g^{-1}) 687, total pore volume (BJH, cm^3 g^{-1}) 0.95, pore diameter (BJH, Å) 49.5. IR (ATR) $\tilde{\nu}$ (cm^{-1}) 3364 (w), 1151 (m), 1035 (s), 1022 (s), 912 (m), 813 (w). UV/Vis (nm) 230, 271, 277. Anal. found C 32.15, H 4.93, S 1.61.

PySO_3-BTEB-PMO (15). The functionalized PMO **14** (0.85 g) was suspended in pyridine (7 mL) and stirred at room temp for 16 h. The light beige solid was filtered off and washed with toluene (3 × 50 mL). To remove some adsorbed residues of pyridine, the solid was stirred for additional 3 h in toluene (18 mL). After the product was filtered off and washed again with toluene (3 × 50 mL), it was dried for 3 h under vacuum to yield 0.75 g of a greyish solid. ^{13}C CP-MAS NMR (125 MHz) δ 131.5, 126.8, 56.4, 52.4, 16.3, 13.7, 10.2. ^{29}Si CP-MAS NMR (99 MHz) δ −62.7, −72.4, −80.6, −92.5, −101.3. PXRD 0.73 (s), 1.36 (w), 1.59 (w). BET $A_{spec.}$ (m^2 g^{-1}) 742, total pore volume (BJH, cm^3 g^{-1}) 0.97, pore diameter (BJH, Å) 52.2. IR (ATR) $\tilde{\nu}$ (cm^{-1}) 3346 (w), 3104 (w), 1632 (w), 1207 (w), 1152 (m), 1041 (s), 1022 (s), 920 (m), 808 (w), 767 (w). UV/Vis (nm) 227, 263, 270, 276. Anal. found C 33.65, H 3.81, N 0.94, S 1.89.

PT1/PT2-BTEB-PMO (16 and 17). In a typical exchange reaction PMO **15** (0.40 g, 211 μmol according to N content) was mixed with phenothiazines **4** or **10** (113 mg, 274 μmol of **4**, 168 mg, 274 μmol of **10**) and suspended in acetonitrile (5 mL). The yellow suspension was stirred at 40 °C for 48 h. The solid was filtered off and washed with acetonitrile (3 × 20 mL) and water (2 × 20 mL). In the last step, the obtained product was dried under vacuum to give 0.37 g respectively 0.39 g of a yellowish solid. **16:** ^{13}C CP-MAS NMR (125 MHz) δ 133.0, 126.6, 115.8, 57.6, 52.1, 22.0, 17.9, 11.8. ^{29}Si CP-MAS NMR (99 MHz) δ −61.5, −71.2, −80.4, −102.4. PXRD 0.64 (s), 1.30 (w), 1.54 (w). BET $A_{spec.}$ (m^2 g^{-1}) 688, total pore volume (BJH, cm^3 g^{-1}) 0.96, pore diameter (BJH, Å) 53.5. IR (ATR) $\tilde{\nu}$ [cm^{-1}] 3374 (m), 3056 (w), 2967 (w), 1635 (w), 1462 (w), 1382 (w), 1151 (m), 1039 (s), 1020 (s), 912 (m). UV/Vis (nm) 228, 256, 270, 276, 299, 520. Anal. found C 36.38, H 3.97, N 1.20, S 2.67. **17:** ^{13}C CP-MAS NMR (125 MHz) δ 140.4, 131.5, 125.6, 114.2, 56.1, 51.0, 16.9, 10.0. ^{29}Si CP-MAS NMR (99 MHz) δ −62.4, −72.0, −80.7, −92.6, −101.4. PXRD 0.69 (s), 1.37 (w), 1.59 (w). BET $A_{spec.}$ (m^2 g^{-1}) 671, total pore volume (BJH, cm^3 g^{-1}) 0.91, pore diameter (BJH, Å) 52.1. IR (ATR) $\tilde{\nu}$ (m^{-1}) 3340 (m), 3059 (w), 1632 (w), 1474 (w), 1382 (w), 1152 (m), 1038 (s), 1022 (s), 918 (m), 809 (w). UV/Vis (nm) 229, 279, 285, 342, 548. Anal. found C 35.74, H 4.03, N 0.82, S 3.50.

Chemical oxidation of PT1-BTEB-PMO (16). 16 (348 mg, 84.6 μmol according to the S content) was degassed at 50 °C for 3 h in vacuum and, after cooling to room temp, suspended in dry dichloromethane (5 mL). After addition of $(NO)BF_4$ (19.7 mg, 169 μmol) the colour changed from beige to raspberry. The solid was filtered off, washed with dichloromethane (3 × 25 mL) and then dried in vacuum. 299 mg of a pink solid was obtained. ^{13}C CP-MAS NMR (125 MHz) δ 132.3, 126.6, 117.9, 68.8, 51.8, 20.7, 17.3, 13.8, 8.8. ^{29}Si CP-MAS NMR (99 MHz) δ −71.6, −80.5, −103.3. PXRD 0.79 (s), 1.74 (w). BET $A_{spec.}$ (m^2 g^{-1}) 467, total pore volume (BJH, cm^3 g^{-1}) 0.60, pore diameter (BJH, Å) 38.3. IR (ATR) $\tilde{\nu}$ (cm^{-1}) 3287 (w), 1381 (w), 1152 (m), 1040 (s), 917 (m), 811 (w), 760 (w). UV/Vis (nm) 234, 272, 276, 298, 341. Anal. found C 34.97, H 3.88, N 0.98, S 2.13.

SH-SBA-15 (19). SBA-15 (**18**) (2.00 g) and 3-MPTS (10.0 g, 48.4 mmol) were suspended in toluene (20 mL) and stirred for 72 h under reflux. After cooling to room temp the product was filtered off, washed with toluene (3 × 50 mL) and dried at 70 °C for 18 h to give 2.31 g of a colourless solid. ^{13}C CP-MAS NMR (125 MHz) δ 45.9, 23.5, 7.4. ^{29}Si CP-MAS NMR (99 MHz) δ −53.9, −63.4, −72.8, −107.9, −116.9. PXRD 0.71 (s) 1.65 (w). BET $A_{spec.}$ (m^2 g^{-1}) 289; total pore volume (BJH, cm^3 g^{-1}) 0.45; pore diameter (BJH, Å) 38.3. IR (ATR) $\tilde{\nu}$ (cm^{-1}) 3357 (w), 2929 (w), 1051 (w), 932 (m), 800 (m), 696 (w). Anal. found C 9.23, H 2.59, S 7.87.

SO_3H-SBA-15 (20). 19 (1.00 g) was suspended in H_2O_2 (35%, 100 mL) and stirred at 60 °C for 24 h. After cooling to room

temp the product was filtered off, washed with water (100 mL) and ethanol (100 mL) and dried at 60 °C for 18 h to give 0.87 g of a colourless solid. ^{13}C CP-MAS NMR (125 MHz) δ 52.8, 17.1, 10.4. ^{29}Si CP-MAS NMR (99 MHz) δ −58.2, −68.1, −102.4, −110.4. PXRD 0.68 (s), 1.61 (w). BET $A_{spec.}$ (m^2 g^{-1}) 581; total pore volume (BJH, cm^3 g^{-1}) 0.75; pore diameter (BJH, Å) 50.5. IR (ATR) $\tilde{\nu}$ (cm^{-1}) 3350 (w), 1637 (w), 1046 (s), 955 (m), 799 (m). Anal. found C 3.26, H 2.32, S 1.97.

PySO$_3$-SBA-15 (21). 20 (0.50 g) was suspended in pyridine (4 mL) and stirred at room temp for 16 h. The light beige product was filtered off and washed with toluene (3 × 50 mL). To remove some adsorbed residues of pyridine the solid was stirred for additional 3 h in toluene (10 mL). After the solid was filtered off and was washed again with toluene (3 × 50 mL), the resulting material was dried for 3 h under vacuum to yield 0.43 g of a greyish solid. ^{13}C CP-MAS NMR (125 MHz) δ 140.9, 126.8, 52.8, 17.1, 10.3. ^{29}Si CP-MAS NMR (99 MHz) δ −58.1, −67.9, −92.5, −101.6, −111.1. PXRD 0.69 (s), 1.41 (w), 1.64 (w). BET $A_{spec.}$ (m^2 g^{-1}) 557; total pore volume (BJH, cm^3 g^{-1}) 0.74; pore diameter (BJH, Å) 50.5. IR (ATR) $\tilde{\nu}$ (cm^{-1}) 3351 (w), 1636 (w), 1041 (s), 957 (m), 797 (m). UV/Vis (nm): 255. Anal. found C 5.58, H 2.08, N 0.76, S 1.96.

PhenoSO$_3$-SBA-15 (22). 21 (0.25 g, 136 μmol according to N content) was mixed with 4 (79.4 mg, 177 μmol) and suspended in acetonitrile (2.4 mL). The yellow suspension was stirred at 40 °C for 48 h. The product was filtered off and washed with acetonitrile (3 × 20 mL) and water (2 × 20 mL). In the last step the resulting material was dried under vacuum to give 0.18 g of a yellow-greyish solid. ^{13}C CP-MAS NMR (125 MHz) δ 143.8, 139.5, 126.5, 115.2, 63.2, 51.6, 42.0, 16.1, 8.7. ^{29}Si CP-MAS NMR (99 MHz) δ −60.2, −66.2, −91.8, −102.9, −111.8. PXRD 0.70 (s), 1.40 (w), 1.64 (w). BET $A_{spec.}$ (m^2 g^{-1}) 448; total pore volume (BJH, cm^3 g^{-1}) 0.65; pore diameter (BJH, Å) 49.1. IR (ATR) $\tilde{\nu}$ (cm^{-1}) 3354 (w), 1049 (s), 960 (m), 801 (m). UV/Vis (nm): 207, 253, 306, 514. Anal. found C 6.96, H 2.01, N 0.73, S 2.52.

3. Results and discussion

3.1. Synthesis and properties of phenothiazinyl alkyl ammonium salts

Immobilization of functional sites on the surface of an inert support material can be realized by three different ways of interaction: (1) adsorption, which in general is a reversible process, (2) covalent binding or (3) electrostatic interaction. In contrast to covalent binding, electrostatic immobilization gives the functional sites more mobility, which can be of benefit for some applications. Here, we report on the electrostatic immobilization of rather large, cationic phenothiazines on a high specific area, periodic mesoporous, BTEB based SBA-15 organosilica material that carries covalently grafted anionic groups. The immobilization process relies on an ion exchange process.

By using this route to a material containing redox-active dye molecules it can be expected that the distribution of the redox centres will be more homogeneous than by applying a classical post-synthetic grafting procedure, where the pores get blocked by the covalent binding of large dye molecules preferentially at the pore entrances. The covalent surface-bound anionic groups required for an electrostatic immobilization of the cationic dye molecules are introduced by small precursors that can diffuse easily into the pores.

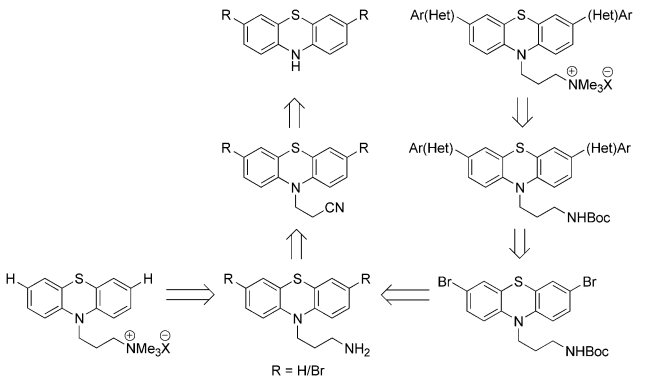

Scheme 1 Retrosynthetic analysis of substituted phenothiazine salts.

To realize this strategy, *N*-alkylated phenothiazines were synthesized bearing quaternary ammonium groups as a counterpart to the anionic species on the scaffold. A retrosynthetic analysis of trimethylammonium substituted phenothiazines suggests the formation of the ammonium salt by the reaction of a primary amine with an alkylating agent (Scheme 1). In case of π-expanded phenothiazines we found that a Boc-protected amine serves as the optimal precursor for the quaternation reaction. For both target compounds, the amine functionality can be introduced by reduction of the corresponding nitrile. Suzuki-cross-coupling reaction seemed to be most suitable for the introduction of (hetero)aryl substituents in the 3,7-positions and the use of a Boc-protected amine as the (hetero)arylhalide source is rational.

A literature known access to cyano substituted phenothiazines is provided by the Michael addition of acrylonitrile to 10*H*-phenothiazine (**1**).[12] Under standard reduction conditions with lithium aluminium hydride in boiling diethyl ether nitrile

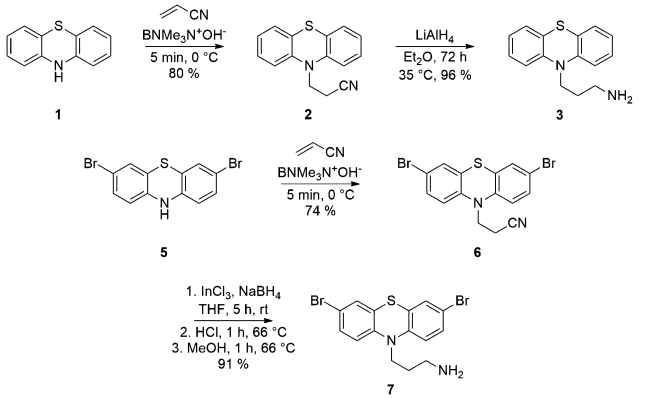

Scheme 2 Syntheses of phenothiazinyl amines **3** and **7**.

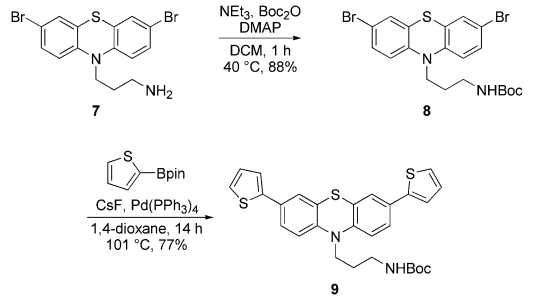

Scheme 3 Synthesis of the dithienylated, Boc-protected, amino alkyl substituted phenothiazine **9**.

2 can be transformed to the corresponding primary amine **3** in excellent yields (Scheme 2).[12]

Based on this procedure the synthesis of π-expanded, dithienylated phenothiazine derivatives with substituents at the 3- and 7-positions was carried out. Starting from **5** the cyanoalkyl chain was introduced. Due to the instability of the cyanoalkyl chain of compound **6** towards strong reducing agents like lithium aluminium hydride an alternative reduction procedure first published by B. Singaram *et al.* was probed.[15] Under rather mild reduction conditions, using indium trichloride and sodium borohydride, the nitrile was transformed into the corresponding amine **7**. After workup of the crude product, the free base amine **7** could be obtained with excellent yield (Scheme 2).

The direct use of the free amine base **7** in the following cross-coupling reaction only led to low yields due to the formation of side products, catalyst deactivation and inefficient column chromatography. However, Boc-protection of the amine group giving compound **8** in almost 90% yield prevented the formation of by-products in the subsequent two-fold thienylation of the phenothiazine core. A Suzuki-coupling protocol turned out to be the best choice for the cross-coupling of the two electron-rich substrates giving compound **9**. The carbon–carbon bond formation was carried out using established reaction conditions from our group with tetrakis(triphenylphosphine)palladium(0) as a catalyst and, due to its good solubility in 1,4-dioxane, caesium fluoride as the base (Scheme 3).

With both derivatives in their amine resp. Boc-protected amine form the generation of the ammonium salts was the next step. Methyl iodide proved to be not suitable for this purpose since the electrochemical oxidation potential of iodide to iodine lies in the same range as for phenothiazine and its derivatives.[16,17] Methyl triflate (MeOTf) has similar reactivity as methyl iodide and it is easy to manage. The amine base **3** reacted smoothly with methyl triflate to give the desired ammonium salt **4** in excellent yield. In terms of the Boc-protected amine **9**, the target compound **10** could be obtained by quantitative deprotection with trifluoroacetic acid (TFA) and subsequent quaternation with methyl triflate (Scheme 4).

The molecular structures of both ammonium salts **4** and **10** were unambiguously supported by spectroscopic characterisation, elemental analysis and HRMS. In their ^{1}H NMR spectra, the ammonium salts **4** and **10** can clearly be identified by the resonances of the trimethylammonium group at δ 3.01 for **4** and δ 3.05 for **10**. In the ^{13}C NMR spectra, the corresponding carbon nuclei resonate at δ 53.3 for compound **4** and at 53.7 for compound **10**. Spectroscopic data of all compounds in this manuscript can be found in the ESI.†

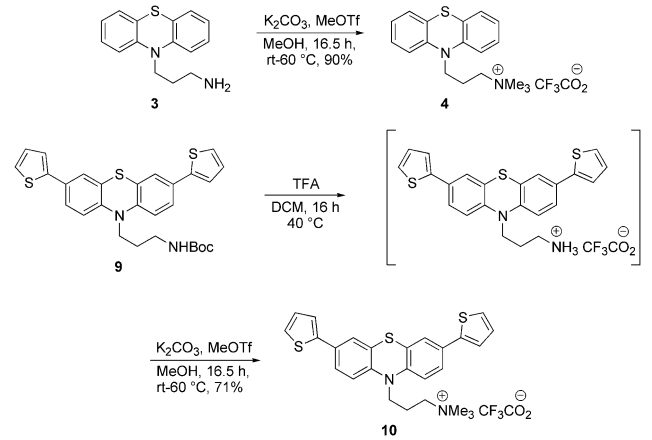

Scheme 4 Syntheses of the alkyl ammonium functionalized phenothiazines **4** and **10**.

Table 1 Selected absorption and emission spectra and CV data of compounds **4** and **10**

Compound	Absorption $\lambda_{max,abs}$/nm (ε 10^3/M^{-1} cm^{-1})	Emission $\lambda_{max,em}$/nm	Stokes shift $\Delta\nu^{-1}$/cm^{-1}	$E_0^{0/+1}$, $E_0^{+1/+2}$/V
4	255 (40), 305 (5)	—	—	0.78
10	289 (53), 342 (18)	489	8800	0.72, 1.26

The electronic properties of the phenothiazinyl ammonium salts **4** and **10** were investigated by absorption and emission spectroscopy and by cyclic voltammetry in the anodic region (up to 1.7 V). The corresponding data are summarized in Table 1. In the absorption spectrum of compound **4** the two typical intense absorption bands of phenothiazine derivatives appear at about 255 nm and 305 nm, representing π–π*-transitions, which was shown by comparison with the unsubstituted phenothiazine.[18,19] No fluorescence was detected for compound **4**.

Compound **10** shows as well two absorption maxima at 289 and 342 nm and furthermore a blue-green fluorescence at 489 nm upon excitation. The emission hardly overlaps with the absorption resulting in a large Stokes shift of 8800 cm^{-1}, which indicates a significant change in the geometry occurring during the transition from the ground state to the excited state.[20] For the evaluation of the oxidation potentials and the reversibility of the first oxidation process cyclic voltammetry measurements were performed in solution. Compound **4** shows the typical behaviour of a quasi-reversible one electron process in the anodic area, with an oxidation potential observed at $E_{ox}^{0/+1}$ = 0.78 V. The cyclic voltammogram of the dithienylated compound **10** shows two well-separated single-electron processes, with oxidation potentials at $E_{ox}^{0/+1}$ = 0.72 V and $E_{ox}^{+1/+2}$ = 1.26 V (see ESI†), the more positive and irreversible process is assigned to the oxidation of one of the thiophene rings.

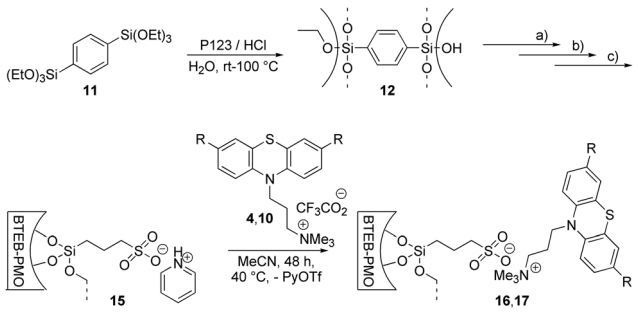

Scheme 5 Synthesis and functionalization of the BTEB based mesoporous material followed by the immobilization of the phenothiazines **4** (R = H) resp. **10** (R = thiophenyl). Conditions: (a) 3-MPTS, toluene, 72 h, reflux; (b) $H_2O_{2(aq.)}$, 24 h, 60 °C; (c) pyridine, 16 h, rt.

3.2. Phenothiazines immobilized on BTEB-PMO as a scaffold.

a. Material synthesis and characterization. As a scaffold for immobilization of the phenothiazines **4** and **10** a BTEB based periodic mesoporous organosilica (**12**) was synthesized from 1,4-dibromobenzene, following modified procedures from the literature.[13,21] The material was subsequently functionalized by post synthetic modification to obtain the pyridinium sulphonate loaded PMO **15** which was then used to immobilize phenothiazines **4** and **10** onto its surface through ion exchange reactions (Scheme 5). For the chemical, structural and textural characterization of **12**, **15**, their intermediates **13** and **14** as well as of the phenothiazine-exchanged products **16** and **17** the typical methods of material chemistry were applied. The complete set of data can again be found in the ESI.†

In its powder XRD, **12** shows the expected *d*(100), *d*(110) and *d*(200) reflexes of a 2D hexagonal *p6mm* structure, typical for SBA-15-like materials.[22] This structure remains pristine throughout the complete modification processes (Fig. 1) which is not the case if ammonia was used instead of pyridine to generate a sulphonate salt containing PMO (see comparison in the ESI†). In addition, SEM images also show a structurally ordered, SBA-15 like material for **16**, even after the whole series of post synthetic modifications (Fig. 1). According to nitrogen physisorption measurements, the specific surface area of 1066 $m^2\ g^{-1}$ for **12** decreases continuously to 688 and 671 $m^2\ g^{-1}$ for **16** or **17**, respectively. All materials show type IV adsorption and desorption isotherms with a large hysteresis which characterizes mesoporous compounds (Fig. 1). The pore size distributions, following the BJH approach, stay stable at around 50 Å over all reaction steps, which already indicates moderate loadings on the material since the pore size should decrease significantly if a high amount of functionalities would have been immobilized inside the pores.

The pore volume decreases by 0.4 $cm^3\ g^{-1}$ throughout the functionalisations while the wall thickness decreases due to a little collapsing in the structure of the material. When **4** and **10** are immobilized, the wall thickness increases by around 2 nm in case of **16** and by about 1 nm for **17**. This difference can be

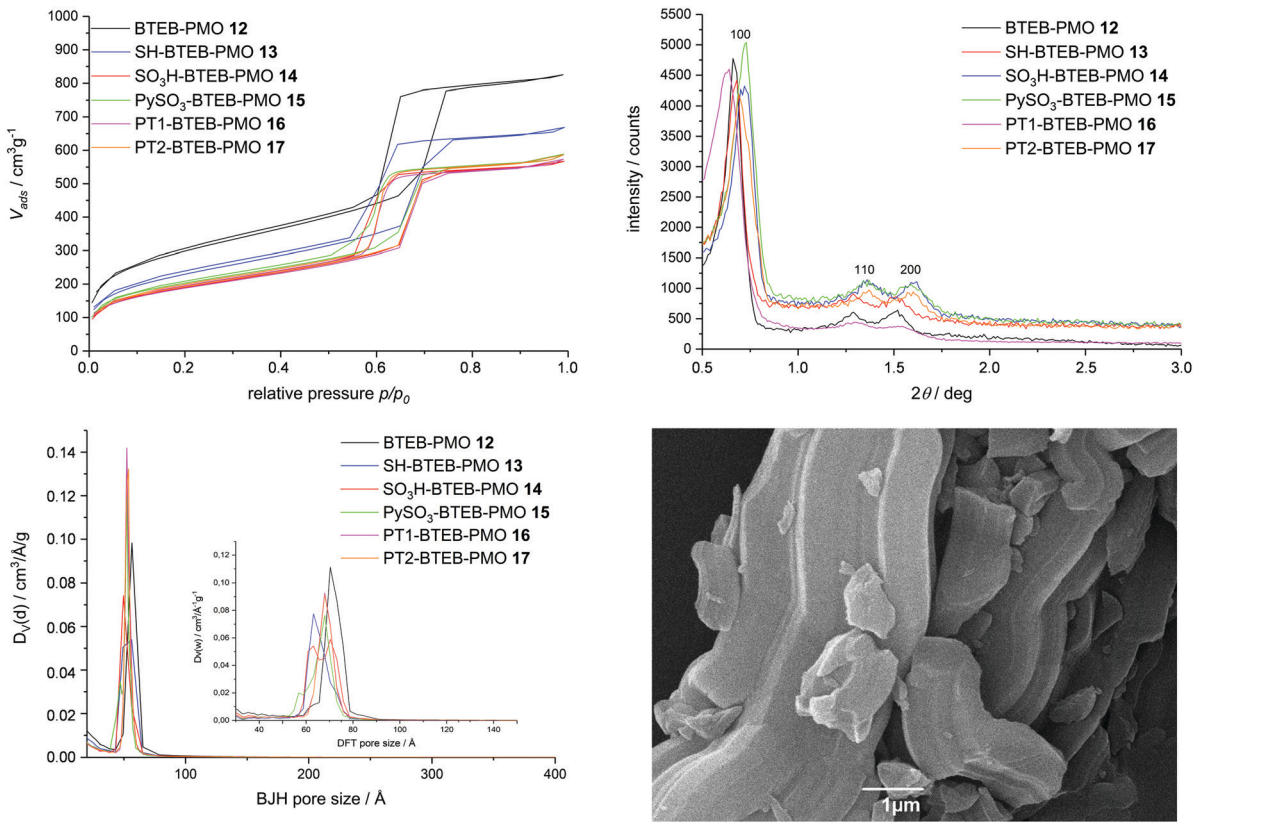

Fig. 1 Powder XRD patterns (top left), nitrogen physisorption isotherms (top right), BJH and DFT pore size distributions (bottom left) and SEM image for **16** as representative (bottom right).

Table 2 Overview of characteristic data for the PMOs (d_{100} is the $d(100)$ spacing, a_0 is the cell parameter ($a_0 = 2d_{100}/\sqrt{3}$), V_p is the pore volume acc. to BJH, $D_{p(BJH)}$ is the average pore diameter according to BJH, w_t is the wall thickness ($a_0 - D_{p(BJH)}$), $A_{spec(BET)}$ is the specific surface area according to BET)

Material	d_{100}/nm	a_0/nm	$V_{p(BJH)}$/cm^3 g^{-1}	$D_{p(BJH)}$/nm	w_t/nm	$A_{spec(BET)}$/m^2 g^{-1}	Loading[a]/μmol g^{-1}
12	13.4	15.4	1.37	5.63	9.77	1066	—
13	13.0	15.0	1.10	5.61	9.39	827	1276
14	12.3	14.2	0.95	4.95	9.25	687	502
15	12.1	14.0	0.97	5.22	8.78	742	589
16	13.8	15.9	0.96	5.35	10.6	688	<461
16$^{\bullet+}$	—	—	0.60	3.83	—	467	<332
17	12.8	14.8	0.91	5.21	9.59	671	<480

[a] Calcd according to the sulphur content of the materials. For the materials containing phenothiazines, the value is a maximum of loading, since it is calculated for a complete ion exchange.

explained by the size of the dyes: **4** is smaller than **10** and therefore it is fitting better into the pores, which leads to a presumably higher loading and finally to an overall thicker wall when **16** and **17** are compared. The data obtained from powder XRD and physisorption measurements for the PMOs are summarized in Table 2.

To prove the successful immobilization, a comparison of the ^{13}C CP-MAS NMR spectra of PMOs **16** and **17** and the high resolution ^{13}C{^{1}H} NMR spectra of the corresponding precursor compounds **4** and **10** is given in Fig. 2. For PMO **16** the signals at δ 115.8 and 22.0 can be assigned to the molecular structure of phenothiazine **4**. Signals that also could be part of the spectrum of **4**, such as the peaks at δ 126.6 and 52.1, are overlapping with peaks that are already present in the ^{13}C CP-MAS NMR of **15**. In the ^{29}Si CP-MAS NMR spectrum of **16**, the three T branches are observed at δ −61.5 (T^1, R-Si(OSi)$_1$(OR′)$_2$), −71.2 (T^2, R-Si(OSi)$_2$(OR′)$_1$) and −80.4 (T^3, R-Si(OSi)$_3$) being typical for silica centres functionalized with aromatic substituents R.[23,24] In addition, a peak at δ −102.4 is present and can be assigned to a Q^3 branch (Si(OSi)$_3$(OR)$_1$) which shows a small destructive effect that occurs during the oxidation process leading to the sulphonic acid intermediate **14** since these silica centres are not anymore connected to a phenylene bridge. In case of **17**, the peaks at δ 140.4 and 114.2 in the ^{13}C CP-MAS NMR have counterparts in the high resolution ^{13}C{^{1}H} NMR spectrum of **10** and therefore prove the immobilisation onto the PMO's surface. Beside the three T branches there are two additional peaks for the scaffold in the ^{29}Si CP MAS NMR spectrum at δ −92.6 and −101.4, which can be assigned to the Q^2 and the Q^3 branch, again originating from the oxidation of the thiol **13**.[10,25]

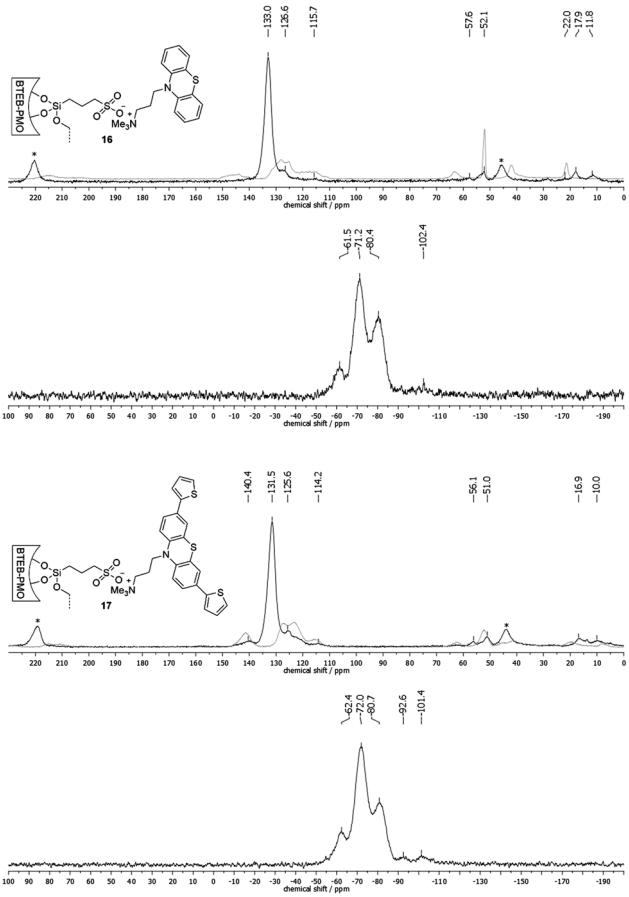

Fig. 2 ^{13}C and ^{29}Si CP-MAS NMR spectra of **16** (top) and **17** (bottom) with high resolution ^{13}C{^{1}H} NMR spectra of **4** and **10** (both grey) for comparison. Rotational sidebands in the ^{13}C spectra are marked with *.

According to elemental analysis, using the sulphur content for calculation, the loading of **4** on **16** is 243 μmol g^{-1} and the loading of **10** on **17** is 167 μmol g^{-1}. This supports the argument given above for the difference of the wall thicknesses since the smaller molecule **4** is fitting better into the pores than **10**. In comparison to our previous work, the loading is lower, caused by the synthetic approach. While in the work of Hemgesberg *et al.* a sol–gel process was applied to synthesize a phenothiazine bearing mesoporous material, we here use post-synthetic grafting followed by ion exchange. The precursors **4** and **10** have to diffuse into already existing pores instead of their concomitant formation with the precursor.[26] Since ion exchange is a typical equilibrium reaction, a complete exchange cannot be expected. This also lowers the loading. Additionally, the aromatic wall of the PMOs lowers the overall loading of the dyes calculated in μmol g^{-1} since the relative mass of the anchoring points is clearly lower than in a neat silica material synthesized from TEOS. One of the strong advantages of the current approach is that phenothiazines are immobilized *via* ionic interactions so that they can hop inside the pores from sulphonate to sulphonate anion, which should lead to a more homogenous distribution of the dyes. Another advantage is the more robust scaffold, coming from the

aromatic walls, which leads to a material that is more tolerable to harsher reaction conditions, overall leading to a material with better ordering.[27,28]

b. Spectroscopy. After successfully immobilizing phenothiazines *via* ionic interaction onto mesoporous organosilicas, the goal was to generate stable radicals on these materials. With **16** two routes were tested: on the one hand **16** was oxidized with $(NO)BF_4$, accordingly to our previous work, to obtain a radical cation with BF_4^- as a counter ion.[26] On the other hand this PMO was stored on a window bench for 24 h since we noticed a colour change when the sample was exposed to daylight. Photo activation of phenothiazines leading to stable radical cations is well known in the literature so that we decided to compare these two strategies.[29] Oxidation with $(NO)BF_4$ leads to a collapse in the structural ordering as can be seen in comparison to the powder XRD and the physisorption data. While the $d(100)$ reflex in the powder XRD shifts to a higher angle, the $d(110)$ and $d(200)$ reflexes completely disappear. Both underline the decrease in structural ordering of the material. In addition, the specific surface area (467 $m^2\ g^{-1}$) is by 221 $m^2\ g^{-1}$ lower than before the chemical oxidation and the pore diameter collapses from 53.5 to 38.3 Å (Fig. 3). Still the reduced structural ordering is not as low as in our previous work demonstrating the robust character of the BTEB based PMO materials.[26] Finally, as the EPR spectra show, the amount of radicals on the material is approximately five times higher upon light exposition (Fig. 3). One reason for this observation is that chemical oxidation causes a loss of immobilized phenothiazine **16** since the loading after the treatment is 332 μmol g^{-1} and therefore approx. 130 μmol g^{-1} lower than prior to oxidation. Furthermore, it might be possible that the collapsed structure resulting from $(NO)BF_4$ treatment has a negative influence on the radical formation. However, over-oxidation of the phenothiazine moiety to the corresponding *S*-oxide should be the most important factor in this context. The *g*-value is in both cases 2.0055 and therefore close to the data of previously reported stable phenothiazine radical cations with g = 2.0051.[30] Also the spectral shape due to the anisotropic unresolved ^{14}N and ^{1}H hyperfine interactions is typical for phenothiazine in a sterically restricted environment.

In the solid state UV/Vis spectra the radical cation is hardly detectable after oxidation with $(NO)BF_4$, while the band at around 540 nm, which can be assigned to the radical, is clearly visible after light irradiation (Fig. 3).[31] A further difference between the two materials is a band at 341 nm appearing after chemical oxidation. A possible explanation for this observation is that the phenothiazine gets over-oxidized, presumably at the sulphur atom, creating a new chromophore. In addition, the visual impression of the sample is different: while irradiation with light leads to an intensely pink material, the one oxidized with $(NO)BF_4$ was only slightly

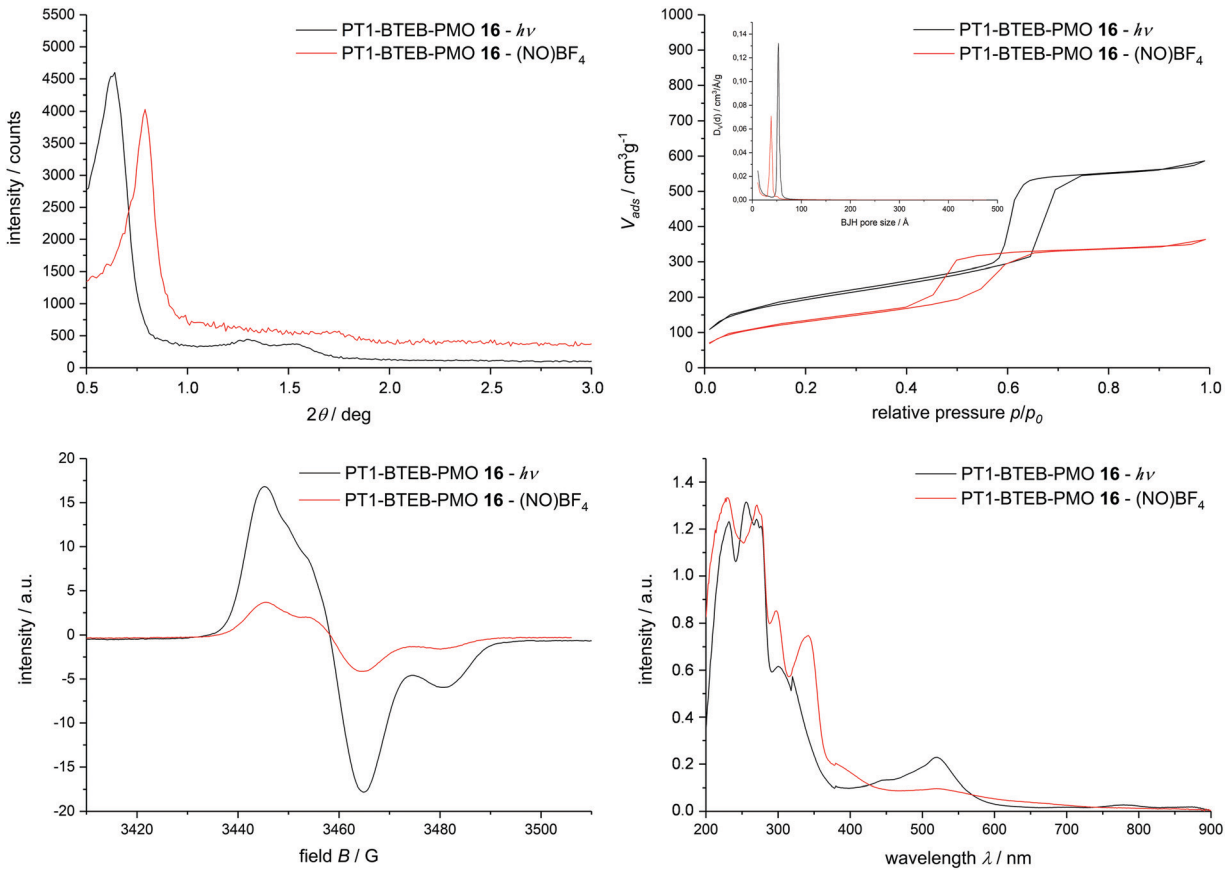

Fig. 3 Powder XRD patterns (top left), nitrogen physisorption isotherms and BJH pore size distributions (top right), EPR spectra (bottom left) and UV/Vis spectra (bottom right) for **16** after treatment with light (black) and $(NO)BF_4$ (red).

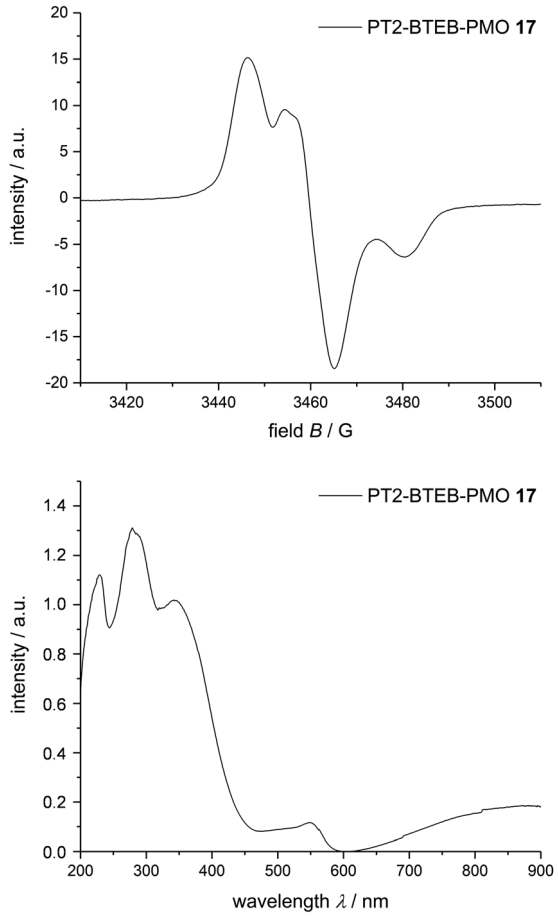

Fig. 4 EPR (top) and UV/Vis spectra (bottom) of **17** after treatment with light.

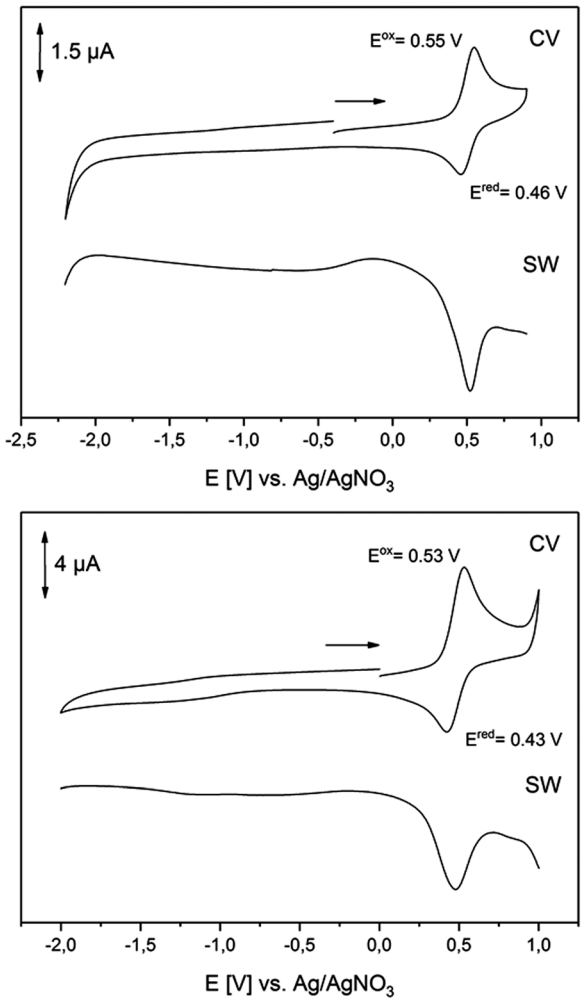

Fig. 5 Cyclic and square-wave voltammograms of **16** (top) and **17** (bottom), measured with a scan rate of 100 mV s^{-1} in a 1 M solution of $^{t}Bu_4NPF_6$ in dichloromethane as electrolyte and with a platinum electrode as working and as counter electrode and a Ag/0.01 M $AgNO_3$/MeCN system as reference electrode.

pink. Pink is the prototypical colour of phenothiazine radical cations.[32]

In case of material **17**, being stored under ambient light the same way as discussed above, there are also radicals formed that can be detected by EPR (*g* value: 2.0047) and by solid state UV/Vis spectroscopy showing a band at 548 nm. The EPR signal is slightly sharper due to the lack of hyperfine couplings of the protons at the 3- and 7-position in compound **17**. This signal becomes rather intense when the PMO was stored under ambient light near by the window bench for 24 h (Fig. 4). In this case, a dusky pink solid results. Both oxidized materials, **16**$^{\bullet+}$ and **17**$^{\bullet+}$, maintain their colour even when they are stored in the dark for ten months, still showing intense signals in the EPR (see the ESI† for comparison), which proves the persistence of the radicals formed. The high stability can be explained by the environment inside the pores. Since not every available pyridinium sulphonate was used for ion exchange (equilibrium reaction), there is still a considerable amount of pyridinium sulphonate inside the pores and, thus, close to the radical cations. These pyridinium sulphonates stabilize the radical cations to a great extent providing them their long-lived character.[31]

In solid state cyclic and square-wave voltammetry measurements of materials **16** and **17** both show a one electron process with a quasi-reversible behaviour (Fig. 5). The oxidation potentials are $E_{ox}^{0/+1}$ = 0.55 and $E_{ox}^{0/+1}$ = 0.53 V for the PMOs, respectively. The second oxidation process of the dithienylated phenothiazine cannot be observed in the solid **17**, an observation that was also reported by Hemgesberg *et al.* with a covalently grafted dithienylated phenothiazine on a SBA scaffold.[26] As the electrochemical data of compounds **4** and **10** were recorded in CH_2Cl_2 suspension, the PMO scaffold provides a more polar environment, rationalizing the slightly lower redox potentials of the phenothiazine sites in the materials **16** and **17** compared to their precursors.

After the generation and analysis of these persistent radicals we took a closer look to the behaviour of material **16**. A sample of **16** was stored in the dark directly after preparation and was then treated under constant UV light, while aliquots were taken after some intervals. These samples were again stored under exclusion of light. Fig. 6 shows the process of radical formation: the intensity of the EPR signal increases over the irradiation time until 24 h were reached. It is also notable that no radicals

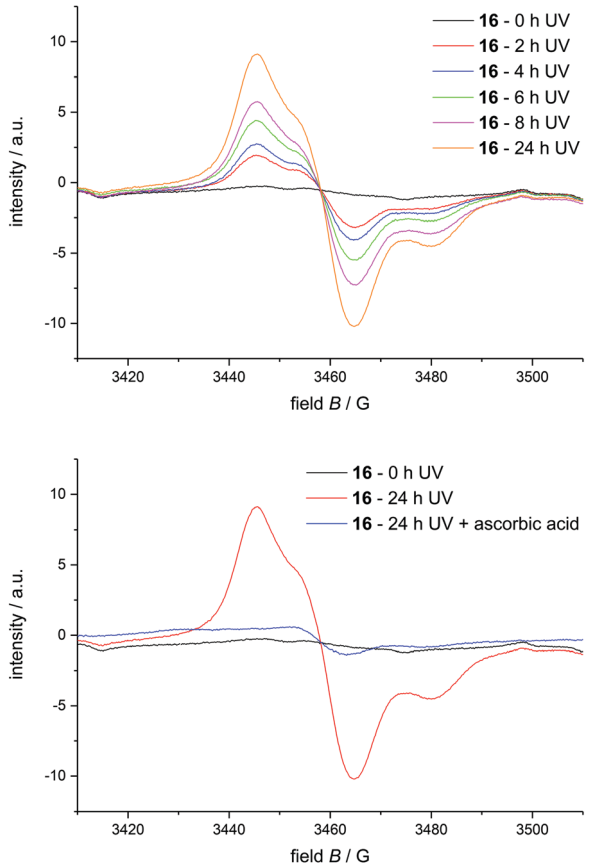

Fig. 6 EPR spectra after different radiation times with UV light (top) and after reduction with ascorbic acid (bottom).

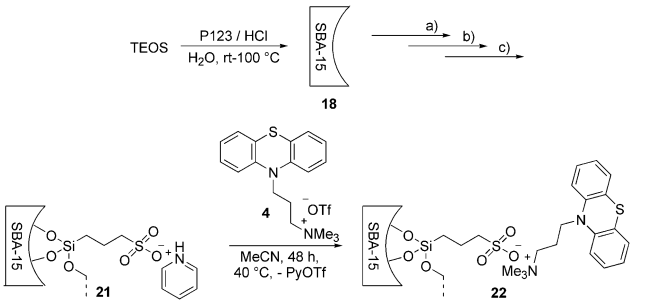

Scheme 6 Synthesis and functionalization of SBA-15 followed by the immobilization of the phenothiazines **4**. Conditions: (a) 3-MPTS, toluene, 72 h, reflux (b) $H_2O_{2(aq.)}$, 24 h, 60 °C (c) pyridine, 16 h, rt.

were found when the freshly prepared sample was directly stored in the dark showing that no radicals are formed during immobilization and that radiation with light is essential to form these radicals. In addition, we tested the reduction of the radical **16**$^{\bullet+}$ with ascorbic acid. Therefore, the material was suspended in a saturated solution of ascorbic acid in degassed water and subsequently washed for several times with degassed water to remove excessive ascorbic acid. The EPR spectrum shows that the radicals nearly disappear due to the reduction indicating the chemical reversibility of the radical formation (Fig. 6). The small residual signal in the EPR spectrum after reduction can be explained with the hydrophobic character of the BTEB-PMOs.[33] It is likely that the aqueous solution of ascorbic acid does not reach every phenothiazine radical in the rather hydrophobic pores so that some of the radical species remain after the reduction process of more accessible radicals.

3.3. Phenothiazines immobilized on SBA-15 as a scaffold

a. Material synthesis and characterization. For exploring whether the aromatic framework of the BTEB-PMOs has more influence on the material properties than a lower loading of phenothiazine, we synthesized the neat silica SBA-15[14] material **18**. This was functionalized the same way as the PMOs (Scheme 6) leading to material **22** loaded with **4**. Again, we obtained the typical 2D hexagonally ordered structure. However, a closer look at the physisorption data shows that there are some differences compared to the organosilica materials. The specific surface area is by 448 $m^2 g^{-1}$ over 200 $m^2 g^{-1}$ lower than for the PMO derivative **16**. Also the average pore size (49.1 Å) is slightly smaller (Fig. 7).

The pore volume decreases significantly when the thiopropyl chains are grafted onto the material indicating the high loading of 2.45 mmol g^{-1}. After oxidation to the sulphonic acid, the pore volume increases since the reaction process leads to a loss of grafted species on the scaffold now possessing a sulphonate loading of 614 μmol g^{-1}. Finally, the pore volume decreases again when compound **4** is immobilized. The wall thickness increases while the grafting procedure, again showing a high content of thiopropyl chains. Thereafter, the wall thickness slightly decreases until the final compound **22** is obtained. The data obtained from powder XRD and physisorption measurements for the SBA-15s are compared in Table 3.

To our surprise the loading of **4** on **22** was only 175 μmol g^{-1} and therefore 68 μmol g^{-1} lower than for PMO **16**. A possible explanation is that on the sulphonate step PMO **15** only contains a slightly lower loading of sulphonate groups with 589 μmol g^{-1} than the SBA-15 **21** with 611 μmol g^{-1}, so the difference before ion exchange is not that as significant as expected. In addition, the PMO derivative **15** has an average pore diameter of 52.2 Å, while neat silica SBA-15 **21** has with 50.5 Å a slightly smaller pore size. The surface area is with 742 $m^2 g^{-1}$ for **15** higher than for **21** with 557 $m^2 g^{-1}$. Finally, the structural ordering is higher for PMOs than for SBA-15s since the *d*(110) and *d*(200) reflexes are hardly detectable in case of the SBA-15s (Fig. 7). In combination, these effects surpass the small difference in sulphonate loading leading to PMO **16** that is with respect to previous aspects superior to the SBA-15 derivative **22**.

b. Spectroscopy. In the EPR and solid state UV/Vis spectra the radical species of **22** is also clearly visible after storage on a window bench (Fig. 8). The *g*-value (2.0056) is nearly the same as for **16**, showing that the difference in the scaffold has virtually no influence on the radical cation.

Therefore the presence of phenylene moieties in the PMO framework is not responsible for the light-driven oxidation of

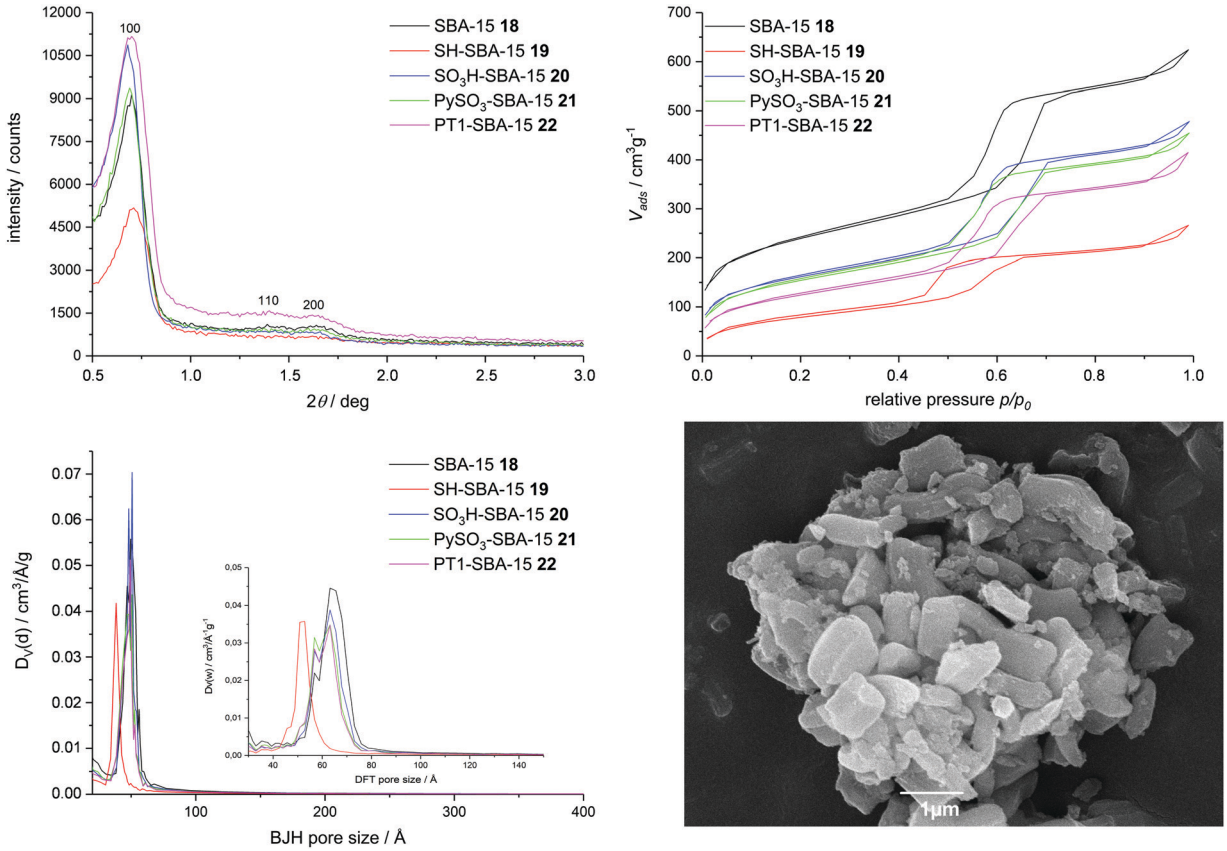

Fig. 7 Powder XRD patterns (top left), nitrogen physisorption isotherms (top right), BJH and DFT pore size distributions (bottom left) and SEM image for **22** as representative (bottom right).

Table 3 Overview over characteristic data for the SBA-15s (d_{100} is the d(100) spacing, a_0 is the cell parameter ($a_0 = 2d_{100}/\sqrt{3}$), V_p is the pore volume, $D_{p(BJH)}$ is the average pore diameter according to BJH, w_t is the wall thickness ($a_0 - D_{p(BJH)}$), $A_{spec(BET)}$ is the specific surface area according to BET)

Material	d_{100}/nm	a_0/nm	V_p/cm^3 g^{-1}	$D_{p(BJH)}$/nm	w_t/nm	$A_{spec(BET)}$/m^2 g^{-1}	Loading[a]/µmol g^{-1}
18	12.6	14.6	0.96	4.94	9.66	840	—
19	12.4	14.4	0.45	3.83	10.6	289	2454
20	13.0	15.0	0.75	5.05	9.95	581	614
21	12.8	14.8	0.74	5.05	9.75	557	611
22	12.6	14.6	0.65	4.91	9.69	448	≥393

[a] Calcd according to the sulphur content of the materials. For the material containing phenothiazines, the value is a maximum of loading, since it is calculated for a complete ion exchange.

the phenothiazines. Since we had not observed a comparable behaviour for the previously published, covalently immobilized systems, we assume that the ionic nature of the phenothiazines clearly favours a rather rapid oxidation under light.

4. Conclusions

Periodic mesoporous organosilica and neat silica materials carrying electrochromophores were obtained by ion exchange reactions with phenothiazine functionalized quaternary ammonium salts. Full characterization of these materials and their organic precursor compounds was carried out. According to UV/Vis spectroscopic data, oxidation of the immobilized phenothiazine centres by applying commonly used (NO)BF_4, resulted in several products of different chemical structure. In contrast, simple irradiation of the phenothiazine containing samples by visible light produced the desired phenothiazine radical cations without any side products. This is in contrast to materials in which the phenothiazine moieties are covalently bound to the surface of mesoporous silica materials. These radical cations are highly stable at room temp and under ambient atmosphere and their formation is not dependent on the support but only on the mode of immobilization. By applying appropriate reducing agents such as ascorbic acid an almost complete regeneration of the neutral phenothiazine sites can be achieved. In combination with solid-state cyclic voltammetry, these experiments prove that the highly reversible redox

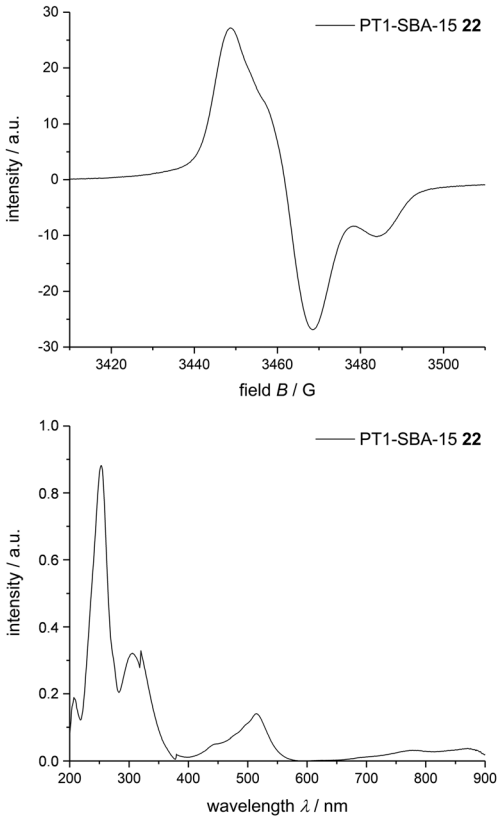

Fig. 8 EPR (top) and UV/Vis spectra (bottom) of **22** after treatment with light.

character of the phenothiazines does not change due to the electrostatic immobilization on inert supports. The results described above now enable a simple access to a broad variety of electrochemically stable, redox-active hybrid materials by ion exchange.

Conflicts of interest

There are no conflicts to declare.

Acknowledgements

The authors wish to thank the Deutsche Forschungsgemeinschaft for financial support of this work (DFG projects MU 1088/13-1 and TH 550/20-1).

Notes and references

1 For a comprehensive review on the chemistry of phenothiazines, see *e.g.* R. A. Aitken and K. M. Aitken, 1,4-Thiazines and their Benzo Derivatives, *Comprehensive Heterocyclic Chemistry III*, 2008, ch. 8.09, vol. 8, p. 607.

2 R. McIntyre and H. Gerischer, *Ber. Bunsen-Ges. Phys. Chem.*, 1984, **88**, 963; G. Diehland and U. Karst, *J. Chromatogr. A*, 2000, **890**, 281; C. Garcia, G. A. Smith, W. G. McGimpsey, I. E. Kochevar and R. W. Redmond, *J. Am. Chem. Soc.*, 1995, **117**, 10871.

3 J. M. Ford, E. P. Bruggemann, I. Pastan, M. M. Gottesman and W. N. Hait, *Cancer Res.*, 1990, **50**, 1748; B. Weiss, W. C. Prozialeck and T. L. Wallace, *Biochem. Pharmacol.*, 1982, **31**, 2217; I. Forrest and F. Forrest, *Biochim. Biophys. Acta*, 1958, **29**, 441; Y. Iida, *Bull. Chem. Soc. Jpn.*, 1971, **44**, 663; J.-C. Moutet and G. Reverdy, *Nouv. J. Chim.*, 1983, **7**, 105; B. Varga, A. Csonka, A. Csonka, J. Molnar, L. Amaral and G. Spengler, *Anticancer Res.*, 2017, **37**, 5983; K. Pluta, B. Morak-Mlodawska and M. Jelen, *Eur. J. Med. Chem.*, 2011, **46**, 3179.

4 S. Taniguchi, N. Suzuki, M. Masuda, S. Hisanaga, T. Iwatsubo, M. Goedert and M. Hasegawa, *J. Biol. Chem.*, 2005, **280**, 7614; E. A. Weinstein, T. Yano, L.-S. Li, D. Avarbock, A. Avarbock, D. Helm, A. A. McColm, K. Duncan, J. T. Lonsdale and H. Rubin, *Proc. Natl. Acad. Sci. U. S. A.*, 2005, **102**, 4548; E. Akoury, M. Pickhardt, M. Gajda, J. Biernat, E. Mandelkow and M. Zweckstetter, *Angew. Chem., Int. Ed.*, 2013, **52**, 3511–3515; E. Nishiwaki, H. Nakagawa, M. Takasaki, T. Matsumoto, H. Sakurai and M. Shibuya, *Heterocycles*, 1990, **31**, 1763; J. Decuyper, J. Piette, M. Lopez, M. P. Merville and A. Vorst, *Biochem. Pharmacol.*, 1984, **33**, 4025; A. G. Motten, G. R. Buettner and C. F. Chignell, *Photochem. Photobiol.*, 1985, **42**, 9; H. Fujita and I. Matsuo, *Chem.-Biol. Interact.*, 1988, **66**, 27.

5 B. Wang, Y. Wang, J. Hua, Y. Jiang, J. Huang, S. Qian and H. Tian, *Chem. – Eur. J.*, 2011, **17**, 2647; R. Y. Lai, X. Kong, S. A. Jenekhe and A. J. Bard, *J. Am. Chem. Soc.*, 2003, **125**, 12631; S. Xu, T. Liu, Y. Mu, Y.-F. Wang, Z. Chi, C.-C. Lo, S. Liu, Y. Zhang, A. Lien and J. Xu, *Angew. Chem., Int. Ed.*, 2015, **54**, 874; E. A. Weiss, M. J. Tauber, R. F. Kelley, M. J. Ahrens, M. A. Ratner and M. R. Wasielewski, *J. Am. Chem. Soc.*, 2005, **127**, 11842; S. Ardo, Y. Sun, A. Staniszewski, F. N. Castellano and G. J. Meyer, *J. Am. Chem. Soc.*, 2010, **132**, 6696; A. Higuchi, H. Inada, T. Kobata and Y. Shirota, *Adv. Mater.*, 1991, **3**, 549; Z.-S. Huang, H. Meier and D. Cao, *J. Mater. Chem. C*, 2016, **4**, 2404; R. S. Nobuyasu, Z. Ren, G. C. Griffiths, A. S. Batsanov, P. Data, S. Yan, A. P. Monkman, M. R. Bryce and F. B. Dias, *Adv. Opt. Mater.*, 2016, **4**, 597; M. Cheng, C. Chen, X. Yang, J. Huang, F. Zhang, B. Xu and L. Sun, *Chem. Mater.*, 2015, **27**, 1808.

6 S. A. Jenekhe, L. Lu and M. M. Alam, *Macromolecules*, 2001, **34**, 7315; X. Kong, A. P. Kulkarni and S. A. Jenekhe, *Macromolecules*, 2003, **36**, 8992; D.-H. Hwang, S.-K. Kim, M. J. Park, J. H. Lee, B. W. Koo, I. N. Kang, S. H. Kim and T. Zyung, *Chem. Mater.*, 2004, **16**, 1298; Y. Zou, W. Wu, G. Sang, Y. Yang, Y. Liu and Y. Li, *Macromolecules*, 2007, **40**, 7231; M. J. Park, J. Lee, J.-H. Park, S. K. Lee, J.-I. Lee, H.-Y. Chu, D.-H. Hwang and H.-K. Shim, *Macromolecules*, 2008, **41**, 3063.

7 M. Hauck, M. Stolte, J. Schönhaber, H. G. Kuball and T. J. J. Müller, *Chem. – Eur. J.*, 2011, **17**, 9984; C. S. Krämer, K. Zeitler and T. J. J. Müller, *Tetrahedron Lett.*, 2001, **42**, 8619; D. Urselmann, K. Deilhof, B. Mayer and T. J. J. Müller, *Beilstein J. Org. Chem.*, 2016, **12**, 2055;

M. Sailer, A. W. Franz and T. J. J. Müller, *Chem. – Eur. J.*, 2008, **14**, 2602; M. Sailer, M. Nonnenmacher, T. Oeser and T. J. J. Müller, *Eur. J. Org. Chem.*, 2006, 423.

8 A. P. Kulkarni, T. W. Kwon and S. A. Jenekhe, *J. Phys. Chem. B*, 2005, **109**, 19584; T. Meyer., D. Ogermann, A. Pankrath, K. Kleinermanns and T. J. J. Müller, *J. Org. Chem.*, 2012, **77**, 3704.

9 N. Bucci and T. J. J. Müller, *Tetrahedron Lett.*, 2006, **47**, 8323; N. Bucci and T. J. J. Müller, *Tetrahedron Lett.*, 2006, **47**, 8329; S. Bay, T. Villnow, G. Ryseck, V. Rai-Constapel, P. Gilch and T. J. J. Müller, *ChemPlusChem*, 2013, **78**, 137.

10 Z. Zhou, A. W. Franz, M. Hartmann, A. Seifert, T. J. J. Müller and W. R. Thiel, *Chem. Mater.*, 2008, **20**, 4986; A. W. Franz, Z. Zhou, R. Turdean, A. Wagener, B. Sarkar, M. Hartmann, S. Ernst, W. R. Thiel and T. J. J. Müller, *Eur. J. Org. Chem.*, 2009, 3895; Z. Zhou, A. W. Franz, S. Bay, B. Sarkar, A. Seifert, P. Yang, A. Wagener, S. Ernst, M. Pagels, T. J. J. Müller and W. R. Thiel, *Chem. – Asian J.*, 2010, **5**, 2001; M. Fingerle, M. Hemgesberg, S. Lach, W. R. Thiel and C. Ziegler, *Thin Solid Films*, 2015, **591**, 8.

11 F. Gai, X. Li, T. Zhou, X. Zhao, D. Lu, Y. Liu and Q. Huo, *J. Mater. Chem. B*, 2014, **2**, 6306; E. Arzoumanian, F. Ronzani, A. Trivella, E. Oliveros, M. Sarakha, C. Richard, S. Blanc, T. Pigot and S. Lacombe, *ACS Appl. Mater. Interfaces*, 2014, **6**, 275.

12 E. F. Godefroi and E. L. Wittle, *J. Org. Chem.*, 1956, **21**, 1163.

13 K. J. Shea, D. A. Loy and O. Webster, *J. Am. Chem. Soc.*, 1992, **114**, 6700.

14 S.-Y. Chen, C.-Y. Tang, W.-T. Chuang, J.-J. Lee, Y.-L. Tsai, J. C. C. Chan, C.-Y. Lin, Y.-C. Liu and S. Cheng, *Chem. Mater.*, 2008, **20**, 3906.

15 J. Z. Saavedra, A. Resendez, A. Rovira, S. Eagon, D. Haddenham and B. Singaram, *J. Org. Chem.*, 2012, **77**, 221.

16 H. Hayashi and T. Koizumi, *Heterocycles*, 2016, **92**, 1441.

17 I. S. El-Hallag, *J. Chil. Chem. Soc.*, 2010, **55**, 67.

18 H. H. Mantsch and J. Dehler, *Can. J. Chem.*, 1969, **47**, 3173.

19 J. E. Bloor, B. R. Gilson, R. J. Haas and C. L. Zirkle, *J. Med. Chem.*, 1970, **13**, 922.

20 L. Yang, J.-K. Feng and A.-M. Ren, *J. Org. Chem.*, 2005, **70**, 5987.

21 B. Schäfgen, O. D. Malter, E. Kaigarula, A. Schüßler, S. Ernst and W. R. Thiel, *Microporous Mesoporous Mater.*, 2017, **251**, 122; S. Shylesh, M. Jia, A. Seifert, S. Adappa, S. Ernst and W. R. Thiel, *New J. Chem.*, 2009, **33**, 717; S. Shylesh, A. Wagener, A. Seifert, S. Ernst and W. R. Thiel, *Angew. Chem., Int. Ed.*, 2010, **49**, 184; F. Rajabi, D. Schaffner, S. Follmann, C. Wilhelm, S. Ernst and W. R. Thiel, *ChemCatChem*, 2015, **7**, 3513.

22 Y. Goto and S. Inagaki, *Chem. Commun.*, 2002, 2410.

23 L. Wang, S. Shylesh, D. Dehe, T. Philippi, G. Dörr, A. Seifert, Z. Zhou, M. Hartmann, R. N. Klupp Taylor, M. Jia, S. Ernst and W. R. Thiel, *ChemCatChem*, 2012, **4**, 395.

24 C. Yoshina-Ishii, T. Asefa, N. Coombs, M. J. MacLachlan and G. A. Ozin, *Chem. Commun.*, 1999, 2539.

25 Z. Zhou, Q. Meng, A. Seifert, A. Wagener, Y. Sun, S. Ernst and W. R. Thiel, *Microporous Mesoporous Mater.*, 2009, **121**, 145–151.

26 M. Hemgesberg, B. Bayarmagnai, N. Jacobs, S. Bay, S. Follmann, C. Wilhelm, Z. Zhou, M. Hartmann, T. J. J. Müller, S. Ernst, G. Wittstock and W. R. Thiel, *RSC Adv.*, 2013, **3**, 8242.

27 N. Mizoshita, T. Tani and S. Inagaki, *Chem. Soc. Rev.*, 2011, **40**, 789.

28 S. Inagaki, S. Guan, Y. Fukushima, T. Ohsuna and O. Terasaki, *J. Am. Chem. Soc.*, 1999, **121**, 9611.

29 N. J. Turro, I. V. Khudyakov and H. van Willigen, *J. Am. Chem. Soc.*, 1995, **117**, 12273; J. Y. Bae, K. T. Ranjit, Z. Luan, R. M. Krishna and L. Kevan, *J. Phys. Chem. B*, 2000, **104**, 9661; J. Y. Bae and L. Kevan, *Microporous Mesoporous Mater.*, 2001, **50**, 1.

30 Y. S. Kang, J. A. Jung and L. Kevan, *J. Chem. Soc., Faraday Trans.*, 1998, **94**, 3247; F. López Rupérez, J. C. Conesa and J. Soria, *Spectrochim. Acta*, 1984, **40**, 1021.

31 M. C. Hovey, *J. Am. Chem. Soc.*, 1982, **104**, 4196.

32 I. Jelínek, I. Němcová and P. Rychlovský, *Talenta*, 1991, **38**, 1309.

33 D. Esquivel, C. Jiménez-Sanchidrián and F. J. Romero-Salguero, *Mater. Lett.*, 2011, **65**, 1460.

